

# SYNCHRONIZATION IN THE COMPLEXIFIED KURAMOTO MODEL\*

HSIAO, TING-YANG<sup>†</sup>, LO, YUN-FENG<sup>‡</sup>, AND WANG, WINNIE<sup>§</sup>

**Abstract.** In this paper, we consider an  $N$ -oscillators complexified Kuramoto model. When the coupling strength  $\lambda$  is strong, sufficient conditions for various types of synchronization are established for general  $N \geq 2$ . On the other hand, we analyze the case when the coupling strength is weak. For  $N = 2$ , when the coupling strength is below a critical coupling strength  $\lambda_c$ , we show that periodic orbits emerge near each equilibrium point, and hence full phase-locking state exists. This phenomenon significantly differentiates the complexified Kuramoto model from the real Kuramoto system, as synchronization never occurs when  $\lambda < \lambda_c$  in the latter. For  $N = 3$ , we demonstrate that if the natural frequencies are in arithmetic progression, non-trivial synchronization states can be achieved for certain initial conditions even when the coupling strength is weak. In particular, we characterize the critical coupling strength ( $\lambda/\lambda_c = 0.85218915\dots$ ) such that a semistable equilibrium point in the real Kuramoto model bifurcates into a pair of stable and unstable equilibria, marking a new phenomenon in complexified Kuramoto models.

**Key words.** Complexified Kuramoto model, Coupled oscillators, Synchronization, Kuramoto model, Lyapunov function, Cherry flow.

**AMS subject classifications.** 34D06, 37C27, 37C20

**1. Introduction.** Synchronization is the natural phenomenon of collective oscillation observed in systems consisting only of autonomous oscillators. This phenomenon has been widely studied since Huygens' Horologium Oscillatorium [23]; for modern studies, we refer readers to the general description materials in [35, 36, 32, 2, 37, 30].

The first attempt at solving this problem came from Winfree [40], who studied the nonlinear dynamics of a coupled system with  $N$  oscillators in the large- $N$  limit via a mean-field approach (see also [35]). Kuramoto refined this model in 1975 [25]. The resulting *Kuramoto model* [26] is a system of weakly coupled, nearly identical, and interacting limit cycle oscillators. For a system of  $N$  oscillators (see, for instance, [39, 24, 31, 1, 5, 34, 22, 11, 21, 4, 10, 9, 6, 7]), the Kuramoto model is a system of  $N$  nonlinear ordinary differential equations (ODEs): for  $n = 1, \dots, N$ ,

$$(1.1) \quad \dot{\theta}_n = \omega_n + \frac{\lambda}{N} \sum_{m=1}^N \sin(\theta_m - \theta_n),$$

where for the  $n$ th oscillator,  $\theta_n$  is its phase angle and  $\omega_n$  its natural frequency. Here, both quantities are assumed to be real.  $\lambda$ , assumed positive, denotes the coupling strength between the  $N$  oscillators.

Recently, researchers have shifted their focus to higher-dimensional interactions and generalized the Kuramoto models by using different algebraic structures. There are many ongoing efforts to further our understanding of the synchronization phenomena through the study of the *Lohe model*, which is a non-Abelian generalization

\*March 3, 2025

**Funding:** None.

<sup>†</sup>International School for Advanced Studies (SISSA), Via Bonomea 265, 34136 Trieste, Italy (thsiao@sissa.it),

<sup>‡</sup>School of Electrical and Computer Engineering, Georgia Institute of Technology, Atlanta, 30332, Georgia, USA (ylo49@gatech.edu),

<sup>§</sup>Department of Physics, University of Wisconsin-Madison, Madison, 53706, Wisconsin, USA (wwang629@wisc.edu).

of the Kuramoto model [28, 12, 19, 20, 33, 13]. Concurrently, there have been ever-increasing interests in the complexified Kuramoto models [18, 38, 27]; more generally, synchronization phenomena in a system of oscillators with complex-valued quantities [17, 3, 8].

Ha et al. first proposed the complexified Kuramoto model [18, Eq. (2.3)] as an example of a general model [18, Eq. (2.1)] for flocking phenomena on an infinite cylinder. The authors also analyzed the behavior of non-identical oscillators when the coupling strength is large enough [18, Assumption (H1)] (what we call “strong coupling” in this work). Moreover, the authors assume that, initially, the spread in the real part ( $x$ ) is strictly smaller than  $\pi/2$ , and that in the imaginary part ( $y$ ) is bounded by some constant dependent on system parameter [18, Assumption (H2)].

Thümler et al. considered the complexified Kuramoto model in the regime of weak coupling [38]. The authors observed that for  $N = 2$  oscillators there exists a conserved quantity (“energy”) when the coupling is weak, and analyzed the system behavior based on this quantity. They also conducted simulations for more than  $N = 2$  oscillators in the weak coupling regime [38, Supplementary Material, Section VI] and observed that solution behavior of the complexified model seems to imply some form of synchronization of the original (real-variable) Kuramoto model.

A follow-up work [27] to [38] considered the complexified Kuramoto model in a new scenario where the coupling strength can take complex instead of real values, which all previous work assumed. The authors analyzed in depth the case of  $N = 2$  complexified Kuramoto oscillators for different cases of the complex coupling strength. They also studied systems of  $N \geq 2$  complexified Kuramoto model and conducted numerical simulations of their behavior.

**1.1. Contributions.** The contributions of this paper are listed below.

1. We further analyze the complexified Kuramoto model proposed in [18]. In particular, based on various regimes of coupling strength to frequency gap ratio, we divide our analysis into “strong coupling” and “weak coupling” cases, and apply different analytical tools for each case. We also define various modes of synchronization to make the meaning of each mode precise.
2. In the “strong coupling” case, many of our proofs analytically verify numerical observations in [38]. For example, numerical observations in [38, Section VI, Supplementary Material] indicate correlations between real and complexified Kuramoto models; some of these correlations are analytically verified by Lemma 3.2 and Theorem 3.4 of this paper.
3. In the “weak coupling” case with  $N = 2$  oscillators, we provide an alternative proof that periodic orbits exist around each equilibrium point. A conserved quantity is constructed in a recent work [38] to characterize these periodic orbits. We further make the interesting observation that full phase-locking synchronization is a sufficient condition for frequency synchronization in the real Kuramoto model, but this is no longer true in the complexified model, with the aforementioned periodic orbits as a counterexample.
4. It is observed numerically and conjectured in [38] that non-trivial phase-locking states exist when the number of complexified Kuramoto oscillators  $N$  is greater than or equal to three. We are the first to analytically prove that non-trivial phase-locking state does exist when  $N = 3$ , even when the coupling strength is weak. Such analysis is generally difficult even for the real Kuramoto models, where most results such as [35, 14, 5, 21] rely on the coupling strength being strong. Notably, our analysis in the “weak coupling”

case (Section 4.2.2) also validates some numerical observations in [29, Fig. 2(b)] for the Cherry flow in real Kuramoto systems. In particular, we get the exact threshold  $\lambda/\omega = \sqrt{\frac{69-11\sqrt{33}}{8}} = 0.85218915\dots$  for the onset of Cherry flow [29, Fig.2(b)].

**1.2. Organization.** We organize the paper in the following order. In Section 2.2, we clarify different levels of synchronization for the complexified Kuramoto model in Definition 2.1-2.3 (see, for instance, [14, 15, 16]). We also introduce a critical coupling strength,  $\lambda_c$ , in Definition 2.4. By using  $\lambda_c$ , we can separate the study of the complexified Kuramoto model into two cases: strong coupling (Section 3) and weak coupling (Section 4).

In Section 3, we consider the case when the coupling strength is strong for  $N \geq 2$  oscillators. Since the real ( $x_n$ ) and imaginary ( $y_n$ ) oscillations can interact with each other (via (2.2)), we first demonstrate the oscillations of both parts individually by alternating the control between the real and imaginary parts. We estimate the difference of the real part between each pair of oscillators (Lemma 3.1). Then, we demonstrate that the oscillators arrive exponentially fast at both frequency and phase synchronization in the imaginary part (Lemma 3.2). Once we achieve this, we demonstrate that the “whole” complexified Kuramoto system (i.e.,  $z(t)$ ) achieves frequency synchronization by using the Lyapunov energy function (3.16) stated in Theorem 3.4. We also prove that, under the same assumptions, the system further achieves phase synchronization if and only if all natural frequencies coincide (Theorem 3.5).

In Section 4, we consider the weak coupling case. The two-oscillators ( $N = 2$ ) case is analyzed in detail in Section 4.1. It is well-known that for classical (real) Kuramoto models with two oscillators, no synchronization can occur when the coupling strength is weak, i.e.,  $\lambda < \lambda_c$ . However, periodic orbits emerge near each equilibrium point in the complexified Kuramoto model. We introduce Lemma 4.1 and use a symmetry argument (Lemma 4.2) to enforce control of the trajectories. Then we observe that a “deceleration region” exists around each equilibrium (Lemma 4.3). Applying these 3 lemmas, we can show that every trajectory is a closed orbit near an equilibrium (Theorem 4.4).

In Section 4.2, we analyze the complexified Kuramoto system with  $N = 3$  oscillators under the “Cherry flow” ansatz in [29]. First, we consider the “super weak” regime, i.e.,  $\lambda < \Lambda_c$ , in Section 4.2.1, where we find that in each  $2\pi$ -period there are two non-real equilibrium points, one a sink and the other a source. The existence of the sink equilibrium further implies that non-trivial initial conditions exist (i.e., start close to the sink) such that the complexified Kuramoto system achieves both full phase-locking and frequency synchronization in this super weak coupling regime. In particular, we develop a simple “horizontal cutting lemma” (Lemma 4.5) to locate two equilibria, and apply the Hartman–Grobman theorem to demonstrate that the stable manifold of both full phase-locking and frequency synchronization exist.

Finally, when the coupling strength  $\lambda$  satisfies  $\Lambda_c \leq \lambda < \lambda_c$  (Section 4.2.2), where we call the coupling strength “weak” but not “super weak” (when  $\lambda = \Lambda_c$ , we say the coupling is “critically weak”), we show that there are full phase-locking states in the complexified system. It is well-known [29] that in real Kuramoto models, semi-stable (“saddle”) equilibrium points exist when the coupling strength is weak. In this paper, we show that as soon as the coupling strength  $\lambda$  exceeds  $\Lambda_c$  in the complexified Kuramoto system, the aforementioned *real* semistable equilibria can *bifurcate* into two equilibria where one is asymptotically stable while the other is unstable, thus demonstrating new synchronization phenomena in the complexified Kuramoto model

versus the real one.

## 2. The complexified Kuramoto model.

**2.1. Preliminaries.** In this paper, we consider a fully-connected network of  $N$  coupled complexified Kuramoto oscillators with  $z_n = x_n + iy_n \in \mathbb{C}$  denoting the angle of the  $n$ th oscillator and  $\omega_i$  its natural frequency. We denote the coupling strength by positive real number  $\lambda$ . Following the complexified Kuramoto model proposed by Thümler, Srinivas, Schröder, and Timme [38], we obtain

$$(2.1) \quad \dot{z}_n = \omega_n + \frac{\lambda}{N} \sum_{m=1}^N \sin(z_m - z_n),$$

or equivalently,

$$(2.2) \quad \begin{cases} \dot{x}_n = \omega_n + \frac{\lambda}{N} \sum_{m=1}^N \sin(x_m - x_n) \cosh(y_m - y_n), \\ \dot{y}_n = \frac{\lambda}{N} \sum_{m=1}^N \cos(x_m - x_n) \sinh(y_m - y_n), \end{cases}$$

for all  $n = 1, 2, \dots, N$ .

It is often useful to introduce a rotating frame by using the changes of the variables

$$(2.3) \quad z_n \mapsto z_n - t(\omega_1 + \dots + \omega_N)/N.$$

This observation may allow us to assume

$$(2.4) \quad \omega_1 + \dots + \omega_N = 0,$$

without loss of generality. Throughout this paper, we assume that the sum of natural frequencies is zero.

**2.2. Definitions of synchronization.** In order to get a clearer understanding of physics described in [38], it is important to distinguish different synchronization concepts.

**DEFINITION 2.1** (Full phase-locking synchronization). *A solution of the complexified Kuramoto model (2.1) achieves full phase-locking if for all  $n, m = 1, \dots, N$ ,*

$$(2.5) \quad \limsup_{t \rightarrow \infty} |z_n(t) - z_m(t)| < \infty.$$

**DEFINITION 2.2** (Frequency synchronization). *A solution of the complexified Kuramoto model (2.1) achieves frequency synchronization if for all  $n, m = 1, \dots, N$ ,*

$$(2.6) \quad \lim_{t \rightarrow \infty} |\dot{z}_n(t) - \dot{z}_m(t)| = 0.$$

**DEFINITION 2.3** (Phase synchronization). *A solution of the complexified Kuramoto model (2.1) achieves phase synchronization if for all  $n, m = 1, \dots, N$ ,*

$$(2.7) \quad \lim_{t \rightarrow \infty} |z_n(t) - z_m(t)| = 0.$$

**DEFINITION 2.4** (Critical coupling strength). *For the complexified Kuramoto model, the critical coupling strength is defined by*

$$(2.8) \quad \lambda_c := \max_{n, m \in \{1, \dots, N\}} |\omega_n - \omega_m|.$$

We pause to remark that Definition 2.2 is equivalent to the following condition

$$(2.9) \quad \lim_{t \rightarrow \infty} |\dot{z}_n(t)| = 0,$$

for all  $n = 1, \dots, N$ , since we assume the mean of natural frequencies is zero in (2.4)<sup>1</sup>. Also, we want to emphasize that in the real Kuramoto model, one can prove that if its solution achieves full phase-locking synchronization, then it also achieves frequency synchronization<sup>2</sup>. However, this is not true in the complexified Kuramoto model, as we will demonstrate in the case for  $N = 2$  when the coupling strength is weak, i.e.,  $\lambda < \lambda_c$ .

### 3. Strong coupling strength.

LEMMA 3.1 (Real part full phase-locking). *Given  $\delta \in (0, \pi)$ , let the coupling strength  $\lambda > \lambda_c / \sin(\delta)$ . Assume that the solution  $(z_1(t), \dots, z_N(t))$  of the complexified Kuramoto model (2.1) satisfies the initial condition  $(x_1(0), \dots, x_N(0)) \in [0, \pi - \delta]^N$ . Then the solution achieves full phase-locking in the real part; in particular, we have*

$$(3.1) \quad |x_n(t) - x_m(t)| < \pi - \delta,$$

for all  $n, m = 1, \dots, N$  and  $t > 0$ .

*Proof.* In the following, we divide the proof into two cases.

In the first case, we assume  $|x_n(0) - x_m(0)| < \pi - \delta$  for all  $n, m = 1, \dots, N$ . We claim that

$$(3.2) \quad |x_n(t) - x_m(t)| < \pi - \delta,$$

for all  $n, m = 1, \dots, N$ , for all  $t \geq 0$ . Suppose, on the contrary, that (3.2) does not hold. It means that there exist a  $t^* > 0$  such that

$$(3.3) \quad |x_n(t^*) - x_m(t^*)| = \pi - \delta, \text{ for some } n, m = 1, \dots, N,$$

and

$$(3.4) \quad \sup_{t \in [0, t^* - \epsilon]} |x_s(t) - x_l(t)| < \pi - \delta,$$

for all  $s, l = 1, \dots, N$ , for all  $0 < \epsilon \ll 1$ . We may assume  $x_n(t^*) - x_m(t^*) > 0$  without loss of generality. Hence, by (3.3) and (3.4), it is clear that  $\dot{x}_n(t^*) - \dot{x}_m(t^*) \geq 0$ . On the other hand, recalling (2.2), we see that

$$\begin{aligned} \dot{x}_n(t) - \dot{x}_m(t) = \omega_n - \omega_m + \frac{\lambda}{N} \sum_{l=1}^N \left( \sin(x_l - x_n) \cosh(y_l - y_n) \right. \\ \left. - \sin(x_l - x_m) \cosh(y_l - y_m) \right). \end{aligned}$$

<sup>1</sup>For  $n = 1, \dots, N$ , we have  $\lim_{t \rightarrow \infty} |\dot{z}_n(t) - \frac{1}{N} \sum_{m=1}^N \dot{z}_m(t)| \leq \lim_{t \rightarrow \infty} \frac{1}{N} \sum_{m=1}^N |\dot{z}_n(t) - \dot{z}_m(t)| = 0$  if the solution achieves frequency synchronization. But  $\sum_{m=1}^N \dot{z}_m(t) \equiv \sum_{m=1}^N \omega_m = 0$ .

<sup>2</sup>Denoting  $H(t) = \sum_{m=1}^N \dot{\theta}_m^2(t)$ , from (1.1), we notice that  $\int_0^t H(s) ds = \sum_{m=2}^N \omega_m(\theta_m(s) - \theta_1(s))|_0^t + \sum_{1 \leq n < m \leq N} \cos(\theta_n(s) - \theta_m(s))|_0^t$ . Also, we observe that  $H(t)$  is uniformly continuous by showing  $\dot{H}$  is bounded. Therefore, the solution achieving full phase-locking synchronization implies the boundedness of  $|\theta_n(t) - \theta_m(t)|$  for all  $n, m = 1, \dots, N$  and all  $t > 0$ , which in turn implies  $\lim_{t \rightarrow \infty} H(t) = 0$ , or equivalently, the solution achieves frequency synchronization.

Therefore, through (3.3), we obtain that, at  $t = t^*$ ,

$$\begin{aligned}
\dot{x}_n - \dot{x}_m &= \omega_n - \omega_m + \frac{\lambda}{N} \sum_{l=1}^N \left( \sin(x_l - x_m - (\pi - \delta)) \cosh(y_l - y_n) \right. \\
&\quad \left. - \sin(x_l - x_m) \cosh(y_l - y_m) \right) \\
(3.5) \quad &\stackrel{(a)}{\leq} \lambda_c + \frac{\lambda}{N} \sum_{l=1}^N \left( \sin(x_l - x_m - (\pi - \delta)) - \sin(x_l - x_m) \right) \\
&\stackrel{(b)}{\leq} \lambda_c - \lambda \sin(\delta) \\
&< 0,
\end{aligned}$$

where (a) is due to  $0 \leq x_l - x_m \leq \pi - \delta$  (this follows from (3.3)) and (b) is due to the inequality  $\sin(x - a) - \sin(x) \leq -\sin(a)$  for  $0 \leq x \leq a < \pi$ . This contradiction then verifies the claim.

For the second case, we assume the initial conditions satisfy  $x_n(0) = \pi - \delta$  and  $x_m(0) = 0$  for some  $n, m = 1, \dots, N$ . Then the inequality (3.5) still holds when  $t = 0$ . Hence, there is some  $t_0 > 0$  such that  $0 < x_n(t) - x_m(t) < x_n(0) - x_m(0) = \pi - \delta$  for all  $t \in (0, t_0]$ . (If there are multiple pairs of  $(n, m)$  satisfying  $x_n(0) = \pi - \delta$  and  $x_m(0) = 0$ , we get  $t_0^{(n,m)} > 0$  for each pair. Then choose  $t_0 = \min_{(n,m)} t_0^{(n,m)} > 0$ .) Then, we can apply the argument in first case to the system (2.2) with the initial condition at  $t = t_0$ .

Therefore, the proof is completed.  $\square$

Our next goal is to analyze the sufficient condition of phase and frequency synchronization for the imaginary part. In order to control the  $y_n - y_m$ , we need to further restrict the quantity for  $x_n - x_m$  for all  $n, m = 1, \dots, N$ .

LEMMA 3.2 (Imaginary part phase and frequency synchronization). *Assume that the solution  $(z_1(t), \dots, z_N(t))$  of the complexified Kuramoto model (2.1) satisfies*

$$(3.6) \quad \limsup_{t \rightarrow \infty} |x_n(t) - x_m(t)| < \frac{\pi}{2} - \delta_0,$$

for all  $n, m = 1, \dots, N$ , for some  $0 < \delta_0 < \pi/2$ . Then the imaginary part of the solution achieves phase and frequency synchronization, i.e.,

$$(3.7) \quad \lim_{t \rightarrow \infty} |y_n(t) - y_m(t)| = 0,$$

and

$$(3.8) \quad \lim_{t \rightarrow \infty} |\dot{y}_n(t) - \dot{y}_m(t)| = 0.$$

Moreover, each convergence is exponentially fast.

*Proof.* Let us define the phase difference function

$$(3.9) \quad Y(t) := \max_{s, l \in \{1, \dots, N\}} |y_s(t) - y_l(t)|$$

for  $t \geq 0$ . It is obvious that  $Y(t) : \mathbb{R}^+ \rightarrow \mathbb{R}$  is a continuous and piecewise smooth function. By (3.6), there exists a  $T > 0$  such that  $|x_n(t) - x_m(t)| < \pi/2 - \delta_0$  for all

$n, m = 1, \dots, N$  and  $t > T$ . Fix any  $t > T$ . There exists a pair  $(n, m) \in \{1, \dots, N\}^2$  such that  $Y(t) = y_n(t) - y_m(t)$ . Recalling (2.2), a straightforward calculation for this phase difference reveals that, at time  $t$ ,

$$\begin{aligned}
 \dot{Y} &= \dot{y}_n - \dot{y}_m \\
 &= \frac{\lambda}{N} \sum_{l=1}^N \left( \cos(x_l - x_n) \sinh(y_l - y_n) - \cos(x_l - x_m) \sinh(y_l - y_m) \right) \\
 &\stackrel{(a)}{\leq} \frac{\lambda \cos(\frac{\pi}{2} - \delta_0)}{N} \sum_{l=1}^N \left( \sinh(y_l - y_n) - \sinh(y_l - y_m) \right) \\
 &\stackrel{(b)}{\leq} \frac{\lambda \sin(\delta_0)}{N} \sum_{l=1}^N \left( (y_l - y_n) - (y_l - y_m) \right) \\
 &\leq -\lambda \sin(\delta_0)(y_n - y_m). \\
 &= -\lambda \sin(\delta_0)Y,
 \end{aligned}$$

where (a) is due to  $y_m \leq y_l \leq y_n$  for all  $l = 1, \dots, N$  and  $|x_l - x_k| < \pi/2 - \delta_0$  for all  $l, k = 1, \dots, N$ ; (b) is due to the mean-value theorem,  $y_m - y_n \leq 0$  and  $\cosh(\cdot) \geq 1$ . With this differential inequality in  $Y$ , thanks to Grönwall's inequality, we obtain

$$(3.10) \quad Y(t) \leq Y(T) \exp(-\lambda \sin(\delta_0)(t - T)),$$

for any  $t > T$ . This means that the imaginary part achieves phase synchronization exponentially fast, so

$$(3.11) \quad \lim_{t \rightarrow \infty} |y_n(t) - y_m(t)| = 0,$$

and hence, frequency synchronization due to (2.2), and thus

$$(3.12) \quad \lim_{t \rightarrow \infty} |\dot{y}_n(t) - \dot{y}_m(t)| = 0.$$

This convergence is also exponentially fast since from (2.2) we have

$$|\dot{y}_n(t)| \leq \lambda \sinh(Y(t))$$

for  $t > T$ . This completes the proof.  $\square$

**THEOREM 3.3 (Full phase-locking).** *Consider the coupling strength and initial conditions described in Lemma 3.1. Then the solution  $(z_1(t), \dots, z_N(t))$  of the complexified Kuramoto model (2.1) achieves full phase-locking.*

*Proof.* By Lemma 3.2, it is sufficient to show  $\limsup_{t \rightarrow \infty} |x_n(t) - x_m(t)|$  is bounded by  $\pi/2$ . In the following, we divide the proof into three cases.

In the first case, we assume  $\delta \in (\pi/2, \pi)$ . By Lemma 3.1, it is clear that

$$|x_n(t) - x_m(t)| < \pi - \delta < \pi/2,$$

for all  $n, m = 1, \dots, N$  and  $t > 0$ , so we are done.

For the second case, assume that  $\delta \in (0, \pi/2)$ . We first note that, if there exists any time instant  $t^* \geq 0$  such that  $|x_n(t^*) - x_m(t^*)| \leq \delta$  for all  $n, m = 1, \dots, N$ , then applying Lemma 3.1 to the system re-started at time  $t^*$  implies that  $|x_n(t) - x_m(t)| \leq \delta < \pi/2$  for all  $n, m = 1, \dots, N$  and  $t \geq t^*$ , thus we will be done.

It remains to show that there indeed exists such a time instant  $t^*$ . We prove this by contradiction: suppose that for all time  $t \geq 0$ ,  $x_{\max}(t) - x_{\min}(t) > \delta$ , where we define  $x_{\max}(t) := \max_{k=1, \dots, N} x_k(t)$  and  $x_{\min}(t) := \min_{k=1, \dots, N} x_k(t)$ .

Fix any time  $t \geq 0$ . For any  $(n, m) \in \arg \max_{k=1, \dots, N} x_k(t) \times \arg \min_{k=1, \dots, N} x_k(t)$ , we have

$$(3.13) \quad \delta < x_n(t) - x_m(t) = x_{\max}(t) - x_{\min}(t) := \beta < \pi - \delta,$$

where the last inequality follows from Lemma 3.1. For any such  $(n, m)$ , a straightforward calculation reveals that

$$(3.14) \quad \begin{aligned} \dot{x}_n(t) - \dot{x}_m(t) &\leq \lambda_c + \frac{\lambda}{N} \sum_{l=1}^N \left( \sin(x_l - x_n) \cosh(y_l - y_n) \right. \\ &\quad \left. - \sin(x_l - x_m) \cosh(y_l - y_m) \right) \\ &\stackrel{(a)}{\leq} \lambda_c + \lambda \max_{x^* \in [\delta, \beta]} \left( \sin(x^* - \beta) - \sin(x^*) \right) \\ &\stackrel{(b)}{\leq} \lambda_c - \lambda \sin(\delta) \\ &< 0. \end{aligned}$$

We pause to remark that (a) is due to (3.13); (b) is due to the function  $\sin(x - \beta) - \sin(x)$ , defined on  $0 \leq x \leq \beta < \pi - \delta$ , achieves its maximum  $-\sin(\beta)$  at  $x = 0$  or  $\beta$ , and from (3.13) we have  $\sin \beta > \sin \delta$ .

This indicates that if  $x_{\max}(t) - x_{\min}(t) > \delta$ , then it is decreasing with the rate of change at least  $\lambda \sin(\delta) - \lambda_c$ , which is a fixed positive value. Thus we have

$$(3.15) \quad x_{\max}(t) - x_{\min}(t) \leq \delta,$$

for  $t \geq T_c := \frac{\pi - 2\delta}{\lambda \sin(\delta) - \lambda_c} > 0$ , which is a contradiction.

Finally, for the third case, we assume  $\delta = \pi/2$ . Then there exists  $\alpha \in (0, \pi/2)$  such that  $\lambda > \lambda_c / \sin(\alpha) > \lambda_c$ . Similarly to the second case, if there exists a time instant  $t^* > 0$  such that  $|x_n(t^*) - x_m(t^*)| \leq \alpha$  for all  $n, m = 1, \dots, N$ , then applying Lemma 3.1 to the system re-started at time  $t^*$  implies that  $|x_n(t) - x_m(t)| \leq \alpha < \pi/2$  for all  $n, m = 1, \dots, N$  and  $t \geq t^*$ , thus we will be done. Then we can prove by contradiction that there indeed exists such a time  $t^*$ , using the same contradiction argument as the second case, with  $\alpha$  in place of  $\delta$ .

The proof is now complete.  $\square$

**THEOREM 3.4** (Frequency synchronization). *Consider the coupling strength and initial conditions described in Lemma 3.1. Then the solution achieves frequency synchronization.*

*Proof.* Based on Lemma 3.2 and Theorem 3.3, the imaginary part of the solution achieves phase and frequency synchronization. It remains to show that the real part also achieves frequency synchronization. We consider an energy function as the following:

$$(3.16) \quad \mathcal{H}(t) := \int_0^t \sum_{n=1}^N \dot{x}_n^2(s) ds.$$



We notice that  $\mathcal{H}(t)$  is an increasing function with respect to  $t$ . The results proved in Lemma 3.2 and Theorem 3.3 imply that  $\dot{x}_n(t)$  and  $\ddot{x}_n(t)$  are bounded, for all  $n = 1, \dots, N$ . Hence,  $\sum_{n=1}^N \dot{x}_n^2(t)$  is uniformly continuous. If  $\mathcal{H}(t)$  is bounded by a time-independent constant, then

$$(3.17) \quad \lim_{t \rightarrow \infty} \sum_{n=1}^N \dot{x}_n^2(t) = 0.$$

Recall the first equation of (2.2) and we arrive at

$$\begin{aligned} & \mathcal{H}(t) \\ &= \int_0^t \left( \sum_{n=1}^N \omega_n \dot{x}_n(s) + \frac{\lambda}{N} \sum_{n,m=1}^N \sin(x_m(s) - x_n(s)) \cosh(y_m(s) - y_n(s)) \dot{x}_n(s) \right) ds \\ &= \sum_{n=1}^N \omega_n (x_n(t) - x_n(0)) \\ &\quad - \frac{\lambda}{N} \sum_{1 \leq m < n \leq N} \int_0^t \sin(x_n(s) - x_m(s)) \cosh(y_m(s) - y_n(s)) (\dot{x}_n(s) - \dot{x}_m(s)) ds \\ &\leq \left| \sum_{n=1}^N \omega_n (x_n(t) - x_n(0)) \right| \\ &\quad + \frac{\lambda}{N} \left| \sum_{1 \leq m < n \leq N} (\cos(x_n(s) - x_m(s)) \cosh(y_m(s) - y_n(s))) \Big|_0^t \right| \\ &\quad + \frac{\lambda}{N} \left| \sum_{1 \leq m < n \leq N} \int_0^t \cos(x_n(s) - x_m(s)) \sinh(y_m(s) - y_n(s)) (\dot{y}_m(s) - \dot{y}_n(s)) ds \right| \\ &=: \mathcal{I}(t) + \mathcal{II}(t) + \mathcal{III}(t). \end{aligned}$$

We want to demonstrate that  $\limsup_{t \rightarrow \infty} (\mathcal{I}(t) + \mathcal{II}(t) + \mathcal{III}(t))$  is bounded by a constant. It is not difficult to directly observe that  $\limsup_{t \rightarrow \infty} \mathcal{II}(t)$  is bounded since cosine is bounded by 1 and  $\limsup_{t \rightarrow \infty} \cosh(y_m(t) - y_n(t)) = \cosh(0) = 1$  due to Lemma 3.2 and Theorem 3.3. Recalling the zero mean assumption for natural frequencies in (2.4), we can obtain the bounds for  $\mathcal{I}(t)$  by

$$\mathcal{I}(t) \leq \sum_{n=2}^N \omega_n |(x_n(t) - x_1(t))| + \sum_{n=2}^N \omega_n |(x_n(0) - x_1(0))|.$$

By Lemma 3.1, we obtain that  $\limsup_{t \rightarrow \infty} \mathcal{I}(t)$  is bounded.

It remains to verify that  $\limsup_{t \rightarrow \infty} \mathcal{III}(t)$  is bounded. Recalling Lemma 3.2 and Theorem 3.3 and (3.12), there exists a  $L > 0$  and  $T_0 > 0$  such that

$$(3.18) \quad |\dot{y}_n(t) - \dot{y}_m(t)| < L,$$

for all  $n, m = 1, \dots, N$  and  $t > T_0$ . Therefore, combining (3.18), Lemma 3.2 and

Theorem 3.3, we obtain

$$(3.19) \quad \begin{aligned} \limsup_{t \rightarrow \infty} \mathcal{III}(t) &\leq \frac{\lambda}{N} \sum_{1 \leq m < n \leq N} \int_0^{T_0} |\sinh(y_m(s) - y_n(s))| |\dot{y}_m(s) - \dot{y}_n(s)| ds \\ &+ \frac{\lambda L}{N} \sum_{1 \leq m < n \leq N} \int_{T_0}^{\infty} \sinh(|y_m(s) - y_n(s)|) ds. \end{aligned}$$

Due to Lemma 3.2, we know that the imaginary part of the solution achieves phase synchronization exponentially fast. Therefore, this implies that the second integration (3.19) is bounded, and hence  $\limsup_{t \rightarrow \infty} \mathcal{III}(t)$  is bounded.

To recapitulate, we have proven that  $\mathcal{H}(t)$  is bounded by a constant which is independent of  $t \in \mathbb{R}^+$ , so the solution  $(z_1(t), \dots, z_N(t))$  of the complexified Kuramoto model (2.1) achieves frequency synchronization. This proof is now complete.  $\square$

**THEOREM 3.5** (Phase synchronization if and only if identical nature frequencies). *Consider the coupling strength and initial conditions described in Lemma 3.1. Then the solution  $(z_1(t), \dots, z_N(t))$  of the complexified Kuramoto model (2.1) achieves phase synchronization if and only if  $\omega_1 = \dots = \omega_N$ .*

*Proof.* First, we show that if  $\omega_1 = \dots = \omega_N$ , then the solution achieves phase synchronization. Recall that we assume  $\sum_{n=1}^N \omega_n = 0$ ; hence  $\omega_1 = \dots = \omega_N = 0$ . By Lemma 3.1 and Lemma 3.2, we know that the differences between imaginary parts, i.e.,  $\{y_n(t) - y_m(t)\}_{1 \leq n, m \leq N}$ , all tend to zero exponentially fast as  $t \rightarrow \infty$  via (3.10). Also, proofs of Theorem 3.3 and Theorem 3.4 imply that the differences between real parts, i.e.,  $\{x_n(t) - x_m(t)\}_{1 \leq n, m \leq N}$ , are bounded by  $\pi/2$  and that the real parts achieve frequency synchronization. Considering all these and taking the limit  $t \rightarrow \infty$  in the first equation of (2.2), we can show that the solutions achieve phase synchronization.

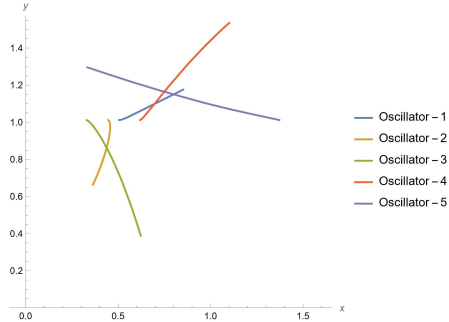
Second, we show that if the solution achieves phase synchronization, then the natural frequencies must coincide; since we assume  $\sum_{n=1}^N \omega_n = 0$ , it suffices to show that  $\omega_1 = \dots = \omega_N = 0$ . For any  $n = 1, \dots, N$ , taking  $t \rightarrow \infty$  in the real-part equation in (2.1) yields  $\omega_n = 0$ , using Theorem 3.4 for the left-hand side, and the phase synchronization assumption on the right-hand side.

This proof is now complete.  $\square$

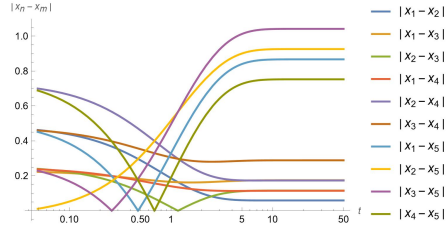
**3.1. Numerical results.** In this subsection, we provide some numerical results to support our analytical conclusions.

In Fig. 1, we demonstrate the time evolution of  $N = 5$  oscillators in the complexified Kuramoto model, for the time duration  $0 \leq t \leq 50$ . We randomly sample  $N = 5$  natural frequencies from the standard normal distribution, then center them so that  $\sum_{n=1}^N \omega_n = 0$ , satisfying the assumption (2.4). We also scale them so that their range is 1, thus  $\lambda_c = 1$  by Def. (2.4). The realization of the natural frequencies for Fig. 1 is, listed as a vector,  $\vec{\omega} := (\omega_1, \dots, \omega_5) = (-0.14, -0.20, -0.32, -0.02, 0.68)$ . Also, we choose the coupling strength  $\lambda = 1.1$  and the parameter  $\delta$  for initial conditions as  $\delta = \pi/2$  (see Lemma 3.1), so that  $\lambda > \lambda_c / \sin(\delta)$  is satisfied, i.e., by definition we are in the *strong coupling* regime. The initial conditions for the real and imaginary parts are sampled independently and uniformly at random from  $[0, \pi - \delta]$ . Note that for the premises of Lemma 3.1 through 3.2 and Theorem 3.3 through 3.4 to hold, we only need the real parts to initially lie in  $[0, \pi - \delta]$ . The realization of the initial conditions in Fig. 1 are, for the real part,  $\vec{x}(0) = (0.85, 0.36, 0.62, 1.10, 0.33)$ , and for the imaginary part,  $\vec{y}(0) = (1.18, 0.66, 0.39, 1.53, 1.30)$ .

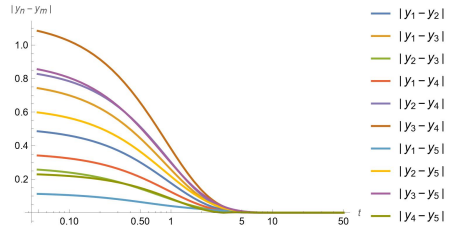
In Fig. 2, the time evolution of  $N = 5$  oscillators with identical natural frequencies in the complexified Kuramoto model, for the time duration  $0 \leq t \leq 50$ . In particular, the natural frequencies  $\vec{\omega} = (0, 0, 0, 0, 0)$  by the assumption (2.4). The other parameters and the initial conditions are chosen to be the same as those in Fig. 1.



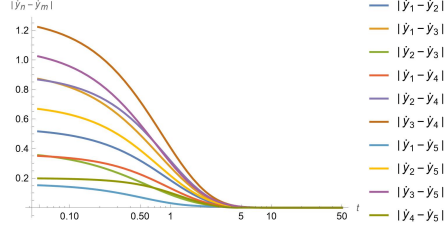
(a) Trajectories  $\{(x_n(t), y_n(t))\}_{1 \leq n \leq 5}$  for the time duration  $0 \leq t \leq 50$ . Frequency synchronization in the imaginary part can be observed, consistent with Lemma 3.2.



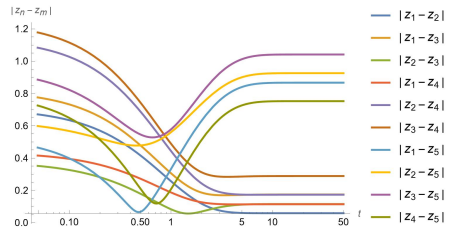
(b)  $\{|x_n(t) - x_m(t)\}_{1 \leq m < n \leq N}$ . Full phase-locking synchronization in the real part can be observed, consistent with Lemma 3.1.



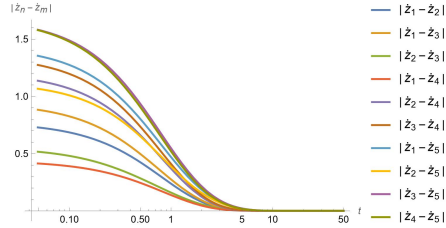
(c)  $\{|y_n(t) - y_m(t)\}_{1 \leq m < n \leq N}$ . Phase synchronization in the imaginary part can be observed, consistent with Lemma 3.2.



(d)  $\{|\dot{y}_n(t) - \dot{y}_m(t)\}_{1 \leq m < n \leq N}$ . Frequency synchronization in the imaginary part can be observed, consistent with Lemma 3.2.

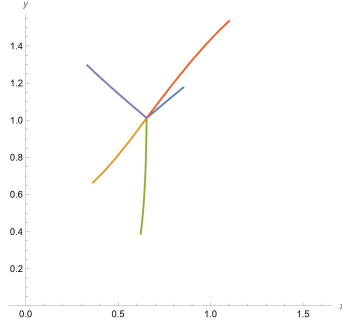


(e)  $\{|z_n(t) - z_m(t)\}_{1 \leq m < n \leq N}$ . Full phase-locking synchronization can be observed, consistent with Theorem 3.3.

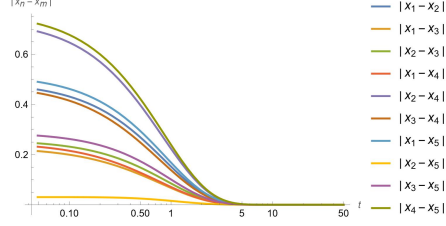


(f)  $\{|\dot{z}_n(t) - \dot{z}_m(t)\}_{1 \leq m < n \leq N}$ . Frequency synchronization can be observed, consistent with Theorem 3.4.

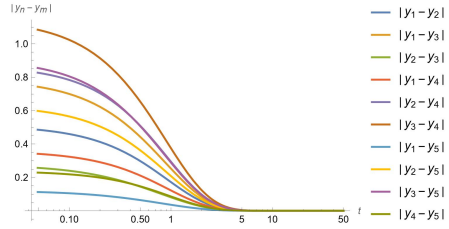
FIG. 1. Time evolution for  $N = 5$  oscillators under strong coupling. See Subsection 3.1 for parameters and initial conditions.



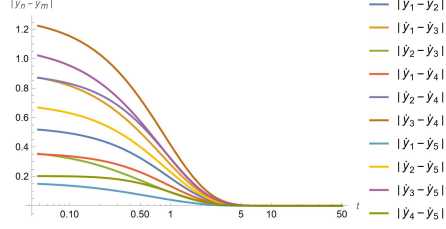
(a) Trajectories  $\{(x_n(t), y_n(t))\}_{1 \leq n \leq 5}$  for the time duration  $0 \leq t \leq 50$ . Phase synchronization can be observed, consistent with Theorem 3.5 (and Theorem 3.3).



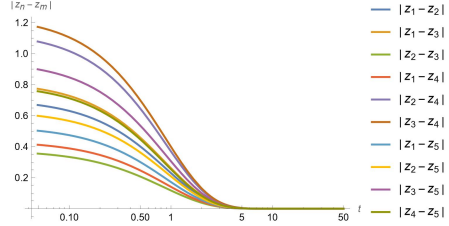
(b)  $\{|x_n(t) - x_m(t)\}_{1 \leq m < n \leq N}$ . Full phase-locking synchronization in the real part can be observed, consistent with Lemma 3.1.



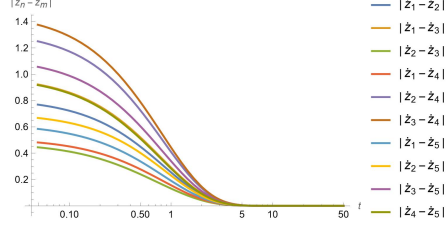
(c)  $\{|y_n(t) - y_m(t)\}_{1 \leq m < n \leq N}$ . Phase synchronization in the imaginary part can be observed, consistent with Lemma 3.2.



(d)  $\{|\dot{y}_n(t) - \dot{y}_m(t)\}_{1 \leq m < n \leq N}$ . Frequency synchronization in the imaginary part can be observed, consistent with Lemma 3.2.



(e)  $\{|z_n(t) - z_m(t)\}_{1 \leq m < n \leq N}$ . Phase synchronization can be observed, consistent with Theorem 3.5 (and Theorem 3.3).



(f)  $\{|\dot{z}_n(t) - \dot{z}_m(t)\}_{1 \leq m < n \leq N}$ . Frequency synchronization can be observed, consistent with Theorem 3.4.

FIG. 2. Time evolution for  $N = 5$  oscillators with identical natural frequencies ( $\omega = \mathbf{0}$ ) under strong coupling. See Subsection 3.1 for parameters and initial conditions.

## 4. Weak coupling strength.

**4.1. Two oscillators.** This subsection will analyze the phase-locking synchronization with the weak coupling strength. We first illustrate this with the two oscillators ( $N = 2$ ) system. Consider two oscillators with  $\omega := 2\omega_1 > 0$  and the weak coupling strength  $\lambda < \omega$ . Define  $x = x_1 - x_2$  and  $y = y_1 - y_2$ . Recall (2.2) and we write

$$(4.1) \quad \begin{cases} \dot{x} = \omega - \lambda \sin(x) \cosh(y), \\ \dot{y} = -\lambda \cos(x) \sinh(y). \end{cases}$$

We pause to remark that it is impossible to arrive at phase-locking synchronization in the real  $N = 2$  Kuramoto model with a weak coupling ( $\lambda < \omega$ ) because there are no fixed points. However, fixed points exist for the complexified Kuramoto model. For instance, one may find fixed points:

$$(x_k, y_k) = \left(2k\pi + \frac{\pi}{2}, \alpha\right),$$

where  $k \in \mathbb{Z}$ ,  $\alpha := \cosh^{-1}(\gamma) = \ln\left(\gamma + \sqrt{\gamma^2 - 1}\right)$  and  $\gamma := \omega/\lambda > 1$ .

In order to state our main theorem for two oscillators system under weak coupling strength we first need to introduce three lemmas that will prove important to the subsequent analysis.

Let us separate the domain near each equilibrium point into four ‘‘quadrants’’ in the  $(x, y)$ -plane as

$$(4.2) \quad Q_{1k} := \left\{ (x, y) \mid x_k < x < x_k + \frac{\pi}{2}, \alpha < y < \infty \right\};$$

$$(4.3) \quad Q_{2k} := \left\{ (x, y) \mid x_k - \frac{\pi}{2} < x < x_k, \alpha < y < \infty \right\};$$

$$(4.4) \quad Q_{3k} := \left\{ (x, y) \mid x_k - \frac{\pi}{2} < x < x_k, 0 < y < \alpha \right\};$$

$$(4.5) \quad Q_{4k} := \left\{ (x, y) \mid x_k < x < x_k + \frac{\pi}{2}, 0 < y < \alpha \right\}.$$

LEMMA 4.1 ( $\delta/n$  criterion). *Assume that the solution  $(x(t), y(t))$  of (4.1) satisfies the initial condition*

$$(4.6) \quad (x(0), y(0)) \in Q_{2k} \cap \left\{ (x, y) \mid \omega - \lambda \sin(x) \cosh(y) = 0 \right\}.$$

*Then, there exists a finite time  $T > 0$  such that*

$$(4.7) \quad (x(T), y(T)) \in \left\{ (x, y) \mid x_k - \frac{\pi}{2} < x < x_k, y = \alpha \right\}.$$

*Proof.* Please see Fig. 3. The proof is given in Appendix 8.1.  $\square$

LEMMA 4.2 (Symmetric property). *Let  $(x(t), y(t))$  be the solution of (4.1) with the initial condition*

$$(4.8) \quad (x(0), y(0)) \in \bigcup_{i=1}^4 cl(Q_{ik}).$$

*Assume that there exists a  $T > 0$ , such that  $x(T) = x_k$  and  $y(T) > 0$ , for some  $k \in \mathbb{Z}$ . Then the trajectory  $(x(t), y(t))$  must exist until at least  $t = 2T$ , and is hence symmetric about the vertical line  $x = x_k$ , when  $0 < t < 2T$ .*

*Proof.* The proof is given in Appendix 8.2.  $\square$

LEMMA 4.3 (Deceleration/Acceleration region). *Given  $k \in \mathbb{Z}$ , let a Lyapunov function be defined as follows:*

$$L_k(x, y) = \frac{1}{2} \left( (x - x_k)^2 + (y - \alpha)^2 \right).$$

There exists an  $\epsilon > 0$ , only depending on  $\alpha$ , such that for every  $k \in \mathbb{Z}$ , the following function

$$F_k(x, y) := \frac{1}{\lambda} \frac{dL_k}{dt} = (x - x_k)(\gamma - \sin(x) \cosh(y)) - (y - \alpha) \cos(x) \sinh(y)$$

is negative on the set  $S_k^-$  and is positive on the set  $S_k^+$ , where

$$S_k^- := \left\{ (x, y) \mid x_k - \frac{\pi}{2} < x < x_k, (1 - \epsilon)\alpha < y < (1 + \epsilon)\alpha \right\},$$

$$S_k^+ := \left\{ (x, y) \mid x_k < x < x_k + \frac{\pi}{2}, (1 - \epsilon)\alpha < y < (1 + \epsilon)\alpha \right\}.$$

*Proof.* The proof is given in Appendix 8.3.  $\square$

With Lemma 4.1-Lemma 4.3 we are ready to prove Theorem 4.4, which gives a sufficient condition for a solution of (4.1) to achieve full phase-locking synchronization.

**THEOREM 4.4.** *Let  $(x, y)$  be a solution of (4.1) under weak coupling strength assumption  $\lambda < \omega$ . Then, every equilibrium point  $(x_k, y_k) = (2k\pi + \pi/2, \alpha)$ , where  $k \in \mathbb{Z}$  is Lyapunov stable but not asymptotically stable, and hence for any solution with initial condition close enough to these equilibria is a periodic orbit.*

*Proof.* First, we focus on the equilibrium point  $(x_0, y_0) = (\pi/2, \alpha)$ , as the analysis for other equilibrium points  $(x_k, y_k)$  are the same via periodicity.

Consider the solution  $(x(t), y(t))$  satisfying the system equations (4.1) with the initial condition

$$(4.9) \quad x(0) = \frac{\pi}{2}, \quad y(0) > \alpha.$$

We observe that the trajectory  $(x(t), y(t))$  must first enter the second quadrant  $Q_{20}$  defined in (4.3), since  $\dot{x}(0) < 0$  and  $\dot{y}(0) = 0$ , and hence fall in  $\{y < y(0)\}$  when  $0 < t \ll 1$ , since  $\dot{y} < 0$  in  $Q_{20}$ . We claim that the trajectory  $(x(t), y(t))$  must hit the curve,  $\omega - \lambda \sin(x) \cosh(y) = 0$  (see the cyan curve in Fig. 4). To prove this, we suppose otherwise that

$$(4.10) \quad (x(0), y(0)) \in \bar{Q}_{20} := Q_{20} \cap \left\{ (x, y) \mid \omega - \lambda \sin(x) \cosh(y) \leq 0, y \leq y(0) \right\}.$$

By Poincaré–Bendixson theorem, either there exists a finite time  $T > 0$  such that  $x(T) = \pi/2$  and  $y(T) > \alpha$  or the asymptotic behaviour of the trajectory satisfies

$$(4.11) \quad (x(t), y(t)) \in \bar{Q}_{20} \text{ when } 0 < t < \infty,$$

and

$$(4.12) \quad \lim_{t \rightarrow \infty} (x(t), y(t)) = \left( \frac{\pi}{2}, \alpha \right).$$

However, it is clear that the trajectory cannot land  $\{x = \pi/2, \alpha < y < y(0)\} \subset \bar{Q}_{20}$ , since  $\dot{x} < 0$  in  $\bar{Q}_{20}$ . Because  $\dot{x} < 0$  in  $\bar{Q}_{20}$ , (4.11) and (4.12) are impossible to be true simultaneously. A contradiction then proves the claim.

Applying the  $\delta/n$  criterion Lemma 4.1, we know that after crossing

$$\omega - \lambda \sin(x) \cosh(y) = 0,$$

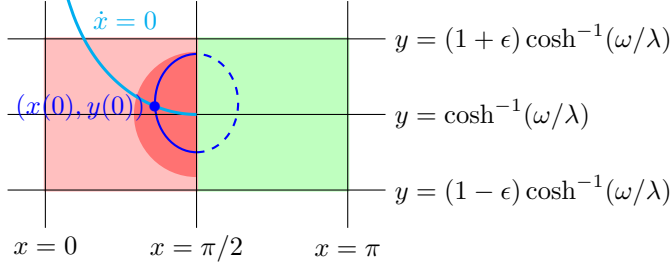


FIG. 3. The trajectory (blue) with initial condition  $(x(0), y(0))$  on the curve  $\dot{x} = 0$  (cyan) will hit the horizontal line  $y = \cosh^{-1}(\omega/\lambda)$ .

the trajectory  $(x(t), y(t))$  will stay at the region  $\tilde{Q}_{20}$  defined in (8.1) until it hits the region

$$(4.13) \quad \left\{ (x, y) \mid 0 < x < \frac{\pi}{2}, y = \alpha \right\}.$$

When it enters this region, we notice that the trajectory then enters the third quadrant  $Q_{30}$ , since  $\dot{y} < 0$  in set (4.13). In  $Q_{30}$ ,  $(x(t), y(t))$  cannot go back to the left boundary  $x = 0$  or swing to the upper boundary  $y = \alpha$ , since  $\dot{x} > 0$  and  $\dot{y} < 0$ . Hence the trajectory either first enter  $\{0 < x \leq \pi/2, y = 0\}$  or  $\{x = \pi/2, 0 < y \leq \alpha\}$ . However, using a symmetry argument from Lemma 4.2 around  $x = \pi/2$ , the trajectory cannot first touch  $\{0 < x \leq \pi/2, y = 0\}$ . This follows from uniqueness ( $y \equiv 0$  is the solution) and the weak coupling case of real Kuramoto. In other words,

$$(4.14) \quad \lim_{t \rightarrow \infty} x(t) = \infty,$$

if  $x(t)$  satisfies the following equation:

$$(4.15) \quad \dot{x} = \omega - \lambda \sin(x).$$

Therefore, the trajectory must pass through  $\{x = \pi/2, 0 < y \leq \alpha\}$ , but not at the fixed point  $(\pi/2, \alpha)$  since  $\dot{y} < 0$  in the third quadrant  $Q_{30}$ .

To recapitulate, we have shown that there exists a time  $\tilde{T} > 0$  such that  $x(\tilde{T}) = \frac{\pi}{2}$  and  $0 < y(\tilde{T}) < \alpha$ . Incorporating the initial condition (4.9) and using Lemma 4.2, we prove that the trajectory  $(x(t), y(t))$  is symmetric to the vertical line  $x = \frac{\pi}{2}$ , and hence form a closed contour. Since the system (4.1) is autonomous, the solution must be periodic with (smallest) period  $2\tilde{T}$ .

To sum up, every solution of the system of equations (4.1) with initial conditions (4.9) is a periodic orbit. To complete the proof of Theorem 4.4, we still have to check whether the equilibrium point  $(\pi/2, \alpha)$  is Lyapunov stable but not asymptotically stable.

Recall Lemma 4.3 and choose  $\epsilon > 0$ . When the initial condition of the system of equations (4.1)  $(x(0), y(0))$ , satisfies

$$(4.16) \quad x(0) = \frac{\pi}{2}, \quad \alpha < y(0) < (1 + \epsilon)\alpha,$$

we have the following

$$\begin{aligned} \dot{x}(0) &= \omega - \lambda \cosh(y(0)) < \omega - \lambda \cosh(\alpha) = 0; \\ \dot{y}(0) &= 0, \end{aligned}$$

so the trajectory  $(x(t), y(t))$  will enter  $Q_{20} \subset S_0^-$  as soon as  $0 < t \ll 1$ .

Then according to the Lyapunov analysis carried out in Lemma 4.3, we have  $dL_0/dt < 0$  on  $S_0^-$ , so the distance of  $(x(t), y(t))$  to the equilibrium point  $(\pi/2, \alpha)$  will strictly decrease as time progresses (until the trajectory leaves  $S_0^-$ ). Equivalently, in the time interval during which the trajectory stays within  $S_0^-$ , the Lyapunov analysis ensures that the trajectory will be confined in the half disk  $\{(x, y) \in S_0^- : (x - \pi/2)^2 + (y - \alpha)^2 \leq (y(0) - \alpha)^2\}$ , shown in Fig. 9 as the dark red region.

By Lemma 4.3, the deceleration region (green area in Fig. 9) to the left of the fixed point implies that  $\alpha - y(\tilde{T}) < y(0) - \alpha$ , which holds for every  $(x(t), y(t))$  and satisfies the system with  $y(0) > \alpha$ . By taking a strictly decreasing sequence of  $y_0^{(n)} \rightarrow \alpha^+$ , one can show that the closed curves (formed by different initial conditions), which must be distinct by uniqueness, form a set of nested contours that are contained one within another and are dense inside the periodic orbit containing  $(x(0) = \pi/2, y(0))$  (see Fig. 4).

To further clarify this argument, we can first choose another  $y_0^{(1)} \in (\alpha, y(0))$  as the starting point. By the above argument, it will produce another periodic orbit. Denote  $u_0^{(1)} \in (0, \alpha)$  as the other  $y$ -coordinate such that this periodic orbit intersects with  $x = \pi/2$  (see Fig. 4). Now, choose any point between these two orbits. Because of the velocity field,  $(\dot{x}, \dot{y})$ , a trajectory starting from this point will also be between these two orbits, without intersecting them. Therefore, the trajectory must touch  $x = \pi/2$  from the right at some finite time and will form a closed loop using Lemma 4.2.

If we are to continue in this manner *ad infinitum*, that is, using a sequence of  $y_0^{(n)} \in (\alpha, y_0^{(n-1)})$  for  $n = 1, 2, 3, \dots$  with  $y_0^{(n)} \searrow \alpha$ , which generates correspondingly a sequence of  $u_0^{(n)} \in (u_0^{(n-1)}, \alpha)$ , it can be shown that except the equilibrium point, any point inside the original periodic orbit lies on another periodic orbit. In particular, the “deceleration region” guaranteed by Lemma 4.3 implies  $0 < \alpha - u_0^{(n)} < y_0^{(n)} - \alpha$ , and thus  $u_0^{(n)} \nearrow \alpha$ . This ensures that the open region  $U^{(n)}$  enclosed by the periodic orbit passing through  $(\pi/2, y_0^{(n)})$  and  $(\pi/2, u_0^{(n)})$  satisfies  $U^{(n)} \supset U^{(n+1)}$  and  $\lim_{n \rightarrow \infty} \mu(U^{(n)}) = 0$  where  $\mu(\cdot)$  stands for Lebesgue measure.

This guarantees that the equilibrium point  $(\pi/2, \alpha)$  is Lyapunov stable but not asymptotically stable. The same above argument may be applied for other equilibrium points  $(x_k, y_k)$  by exploiting the periodicity. This completes the proof.  $\square$

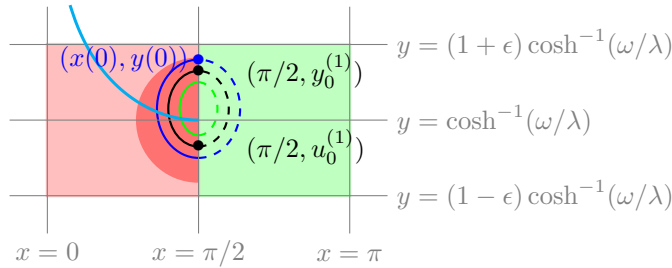


FIG. 4. Inside the blue trajectory with initial condition  $(x(0), y(0))$ , the black trajectory with initial condition  $(\pi/2, y_0^{(1)})$  also forms a closed loop via the same argument. Denote  $(\pi/2, u_0^{(1)})$  as the other intersection point of the black trajectory with the line  $x = \pi/2$ . Similarly, the green trajectory with initial condition  $(\pi/2, y_0^{(2)})$  forms a closed loop inside the black trajectory, and so on *ad infinitum*.



**4.2. Three oscillators.** In this subsection, we demonstrate that synchronization can be achieved in the case  $N = 3$  under weak coupling strength by imposing a *Cherry flow*-type ansatz, i.e., we assume the following two conditions in (2.1) or equivalently (2.2):

1.  $\omega_1 - \omega_2 = \omega_2 - \omega_3 > 0$ . (The natural frequencies are in arithmetic progression.)
2.  $z_1(0) - z_2(0) = z_2(0) - z_3(0)$ . That is,
  - $x_1(0) - x_2(0) = x_2(0) - x_3(0)$ .
  - $y_1(0) - y_2(0) = y_2(0) - y_3(0)$ .

We call this a *Cherry flow*-type ansatz since it is a complexified version of the Cherry flow scenario in the real Kuramoto model, see, e.g., [29, Eq. (3)], where it is argued that the existence of full phase-locking states of the “general” (i.e., without assumptions on parameter values and initial states)  $N$ -oscillator Kuramoto system are difficult to guarantee, due to the difficulty of solving  $N$  coupled non-linear equations.

Notice that the set of possible solutions satisfying the *Cherry flow*-type ansatz above constitutes an invariant manifold based on uniqueness of solution. In particular, we have that for all  $t \geq 0$ ,  $z_1(t) - z_2(t) = z_2(t) - z_3(t)$ . Thus, one may denote

$$\begin{aligned} x(t) &:= x_1(t) - x_2(t), \\ y(t) &:= y_1(t) - y_2(t), \\ \omega &:= \omega_1 - \omega_3 = 2(\omega_1 - \omega_2). \end{aligned}$$

and rewrite (2.2) as

$$(4.17) \quad \begin{cases} \dot{x} = \frac{\omega}{2} - \frac{\lambda}{3}(\sin(x) \cosh(y) + \sin(2x) \cosh(2y)), \\ \dot{y} = -\frac{\lambda}{3}(\cos(x) \sinh(y) + \cos(2x) \sinh(2y)). \end{cases}$$

Notice that in this case,  $\omega = \lambda_c$  where  $\lambda_c$  is defined in (2.8). Let us define three regimes of weak coupling:

1. Super weak:  $\lambda < \Lambda_c := 3\omega / (2 \max_{x \in \mathbb{R}}(\sin(x) + \sin(2x))) = \sqrt{\frac{69-11\sqrt{33}}{8}}\omega = 0.85218915\dots\omega$ .
2. Critically weak:  $\lambda = \Lambda_c$ .
3. Weak:  $\Lambda_c < \lambda < \lambda_c = \omega$ .

**4.2.1. “Super weak” case  $\lambda < \Lambda_c$ .** In this part, we show that under the “super weak” assumption, the system of equations (4.17) possess two equilibria in each set:

$$(4.18) \quad R_k := \left\{ (x, y) \mid 2k\pi \leq x < 2(k+1)\pi, y \geq 0 \right\},$$

where  $k \in \mathbb{Z}$ , and moreover, one of these equilibria is a stable equilibrium  $(x^k, y^k)$  and the other is an unstable equilibrium  $(\bar{x}^k, \bar{y}^k)$ . We restrict our attention to  $y \geq 0$  since it is clear from the system equation (4.17) that if  $(x(t), y(t))$  is a solution, so is  $(x(t), -y(t))$ .

Due to the periodicity of the system in the real component, without loss of generality, we focus on the equilibria in the set  $R_0$ . Before analyzing the stability of each equilibrium point, we first need to locate them, i.e., they are roots of the following

system of non-linear equations:

$$(4.19) \quad \begin{cases} \frac{\omega}{2} - \frac{\lambda}{3}(\sin(x) \cosh(y) + \sin(2x) \cosh(2y)) = 0, \\ -\frac{\lambda}{3}(\cos(x) \sinh(y) + \cos(2x) \sinh(2y)) = 0. \end{cases}$$

In the following, we first derive a necessary condition for the real part of equilibrium points via a root-finding argument for a polynomial equation in the variable  $\sin(2x)$ . Then, we develop Lemma 4.5, analogous to root-finding for single variable continuous functions, for bi-variate continuous functions to locate possible equilibrium points of system (4.19). We then use the previous necessary condition to rule out invalid candidates.

First, we observe that  $y = 0$  cannot be a solution of system (4.19) when the coupling strength is super weak  $\lambda < \Lambda_c$ , by definition. Using hyperbolic function identities, the second equation in system equations (4.19) yields

$$(4.20) \quad \cos(x) + 2 \cos(2x) \cosh(y) = 0.$$

By (4.20), we obtain

$$(4.21) \quad \cosh(y) = -\frac{\cos(x)}{2 \cos(2x)},$$

which is well-defined, since  $\cos(2x)$  cannot be zero; otherwise, via (4.20) we have  $\cos(x) = 0$ , which further implies  $\cos(2x) = 2 \cos^2(x) - 1 = -1$ , contradicting  $\cos(2x) = 0$ .

Recalling the hyperbolic function identities for  $\cosh(2y)$  and substituting equation system equations (4.21) into first equation in (4.19), we arrive at

$$(4.22) \quad \frac{3\omega}{2\lambda} = \sin(x) \left( -\frac{\cos(x)}{2 \cos(2x)} + 2 \cos(x) \left( \frac{\cos^2(x)}{2 \cos^2(2x)} - 1 \right) \right).$$

We exploit the trigonometric identities and make a straightforward calculation to obtain

$$(4.23) \quad 4 \sin^3(2x) + \frac{6\omega}{\lambda} \sin^2(2x) - 3 \sin(2x) - \frac{6\omega}{\lambda} = 0.$$

Let the cubic polynomial having a root  $\sin(2x)$  be

$$(4.24) \quad p(x) = 4x^3 + \frac{6\omega}{\lambda}x^2 - 3x - \frac{6\omega}{\lambda}.$$

We observe that  $p(-1) = -1 < 0$  and  $p(1) = 1 > 0$ , hence there exists at least one real root of  $p(x)$  in  $(-1, 1)$ . Also, we have that  $p'(-1) = 12(1 - \omega/\lambda) - 3 < 0$  (since weak coupling,  $\lambda > \omega$ ) and that leading coefficient of  $p$  is positive), hence there can only be one real root of  $p(x)$  in  $(-1, 1)$ . We can further locate this real root in  $(0, 1)$  since  $p(1) = 1 > 0$  and  $p(0) = -6\omega/\lambda < 0$ . In summary, we have derived a necessary condition for any real part  $x$  of an equilibrium point in system (4.19), namely, that  $\sin(2x) \in (0, 1)$ .

LEMMA 4.5 (Horizontal cutting lemma). *Consider a continuous function  $f : \mathbb{R}^2 \rightarrow \mathbb{R}$ . Let  $g_1 : [y_1, y_2] \rightarrow \mathbb{R}$  and  $g_2 : [x_1, x_2] \rightarrow \mathbb{R}$  be two strictly monotone*

continuous functions such that  $g_1(y_1) = g_2(x_1)$  and  $g_1(y_2) = g_2(x_2)$ . If  $f(x_1, y_1) \cdot f(x_2, y_2) < 0$ , then the system of equations:

$$(4.25) \quad \begin{cases} f(x, y) = 0, \\ g_2(x) - g_1(y) = 0, \end{cases}$$

has at least one root  $(\tilde{x}, \tilde{y})$ , and hence  $x_1 < \tilde{x} < x_2$  and  $y_1 < \tilde{y} < y_2$ .

*Proof.* Let the continuous function  $G$  defined by  $G(x) = g_1^{-1}g_2(x)$ . Clearly, because of intermediate value theorem,  $G : [x_1, x_2] \rightarrow [y_1, y_2]$  is well-defined. Therefore, we obtain  $f(x_1, G(x_1)) \cdot f(x_2, G(x_2)) < 0$ . Using the intermediate value theorem again, we complete the proof.  $\square$

To apply Lemma 4.5 to our system 4.19, let

$$(4.26) \quad f(x, y) := \frac{3\omega}{2\lambda} - (\sin(x) \cosh(y) + \sin(2x) \cosh(2y))$$

be defined on  $(x, y) \in \mathbb{R}^2$ , let

$$(4.27) \quad g_1(y) := 2 \cosh(y)$$

be defined on  $\mathbb{R}^+$  and let

$$(4.28) \quad g_2(x) := -\frac{\cos(x)}{\cos(2x)}$$

be defined on the domain

$$(4.29) \quad \begin{aligned} & \{x \in [0, 2\pi) : -\frac{\cos(x)}{\cos(2x)} \geq 2\} \\ & = \left(\frac{\pi}{4}, r_1\right] \cup \left(\frac{3\pi}{4}, r_2\right] \cup \left[r_3, \frac{5\pi}{4}\right) \cup \left[r_4, \frac{7\pi}{4}\right), \end{aligned}$$

where  $r_l$ ,  $l = 1, 2, 3, 4$  satisfies  $g_2(r_l) = g_1(0) = 2$  and  $\pi/4 < r_1 < 3\pi/4 < r_2 < \pi < r_3 < 5\pi/4 < r_4 < 7\pi/4$  (see Fig. 5). By observing Fig. 5, we can see that for any  $y > 0$ , there are exactly *four* corresponding  $x$ -values for which  $g_1(y) = g_2(x)$  (which is equivalent to the second equation in (4.19)), one in each interval in (4.29). To further locate  $r_l$ , we observe that  $r_l$ 's satisfying the equation  $g_2(r_l) = 2$  can be solved exactly as

$$(4.30) \quad r_1 = \arccos\left(\frac{-1 + \sqrt{33}}{8}\right), \quad r_2 = \arccos\left(\frac{-1 - \sqrt{33}}{8}\right),$$

$$(4.31) \quad r_3 = 2\pi - \arccos\left(\frac{-1 - \sqrt{33}}{8}\right), \quad r_4 = 2\pi - \arccos\left(\frac{-1 + \sqrt{33}}{8}\right).$$

It is straightforward to see that  $\sin(2x) < 0$  when  $x \in (\frac{3\pi}{4}, r_2] \cup [r_4, \frac{7\pi}{4})$ . By the necessary condition  $\sin(2x) \in (0, 1)$  that we derived for the real part of any equilibrium above, we conclude that no equilibrium can have its real part in these two intervals.

Next, we apply Lemma 4.5 on the domains  $(\frac{\pi}{4}, r_1]$  or  $[r_3, \frac{5\pi}{4})$  respectively (observe via Fig. 5 that  $g_2(x)$  is monotonic restricted to each) to ensure that there exists

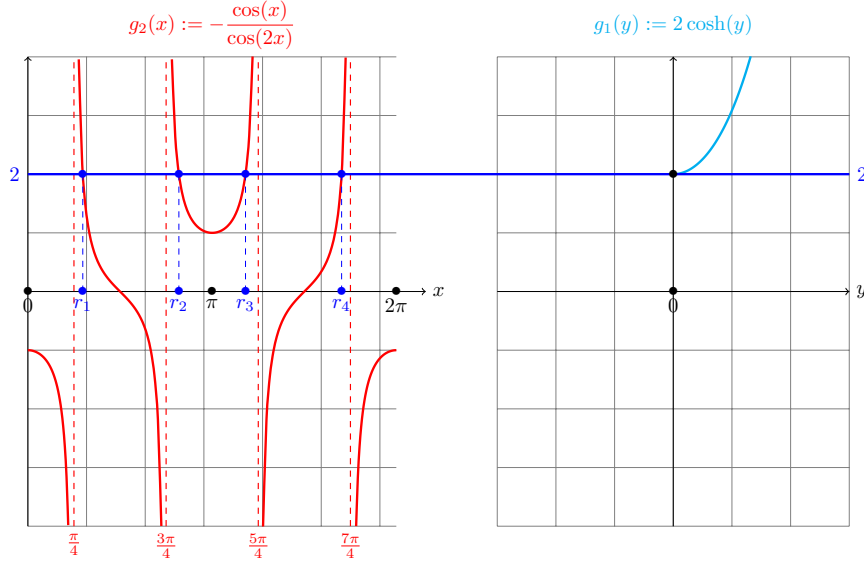


FIG. 5. These two plots are illustrations of Lemma 4.5 for the specific functions  $g_1(y)$  (right) and  $g_2(x)$  (left). The indigo line shows that for  $l = 1, 2, 3, 4$ ,  $g_2(r_l) = g_1(0) = 2$ .

equilibria whose real component lie in those intervals. By a direct calculation, we have

$$(4.32) \quad f(r_1, 0) = \frac{3\omega}{2\lambda} - \sin(r_1) - \sin(2r_1) = \frac{3\omega}{2\lambda} - \max_{x \in \mathbb{R}}(\sin(x) + \sin(2x)),$$

$$(4.33) \quad f\left(\left(\frac{\pi}{4}\right)^+, \infty\right) = -\infty.$$

The second equality in (4.32) can be seen via Fig. 6, noting that  $g_2(x) = 2$  if and only if  $h'(x) = 0$ , where  $h(x) := \sin(x) + \sin(2x)$ . From (4.32) we have  $f(r_1, 0) > 0$  in the super weak regime, by definition. Hence by means of (4.32), (4.33) and Lemma 4.5, we ensure that there exists at least one  $\tilde{x}_1 \in (\pi/4, r_1)$ ,  $\tilde{y}_1 > 0$  such that  $(\tilde{x}_1, \tilde{y}_1)$  is a root for system of equations (4.19). From Fig. 5 we further conclude that there are no other roots in  $R_0$  for which the real part lies in the same interval  $(\pi/4, r_1]$ .

Applying the same procedure to search the interval  $[r_3, 5\pi/4)$ , we have

$$(4.34) \quad f(r_3, 0) = \frac{3\omega}{2\lambda} - \sin(r_3) - \sin(2r_3) \approx \frac{3\omega}{2\lambda} - 0.369 > 0,$$

$$(4.35) \quad f\left(\left(\frac{5\pi}{4}\right)^-, \infty\right) = -\infty.$$

(Notice that via (4.34), even in the “super weak” and the “weak” regimes, we still have  $f(r_3, 0) > 0$ .) Combining (4.34), (4.35) and Lemma 4.5, it is immediate that there exists a *unique* pair  $\tilde{x}_3 \in (r_3, 5\pi/4)$ ,  $\tilde{y}_3 > 0$  such that  $(\tilde{x}_3, \tilde{y}_3)$  is a root for system of equations (4.19).

To recapitulate, we proved that system equations (4.17) only have two equilibrium points in  $R_0$ , where one of them has its real component in  $(\pi/4, r_1)$  and the other in  $(r_3, 5\pi/4)$ .

Next, to analyze (asymptotic) stability of these equilibria, we linearized the system equations (4.17) about  $(\tilde{x}_l, \tilde{y}_l)$ ,  $l = 1, 3$ , we arrive at

$$(4.36) \quad \begin{pmatrix} \dot{x} \\ \dot{y} \end{pmatrix} = \begin{pmatrix} L_{11}(\tilde{x}_l, \tilde{y}_l) & L_{12}(\tilde{x}_l, \tilde{y}_l) \\ L_{21}(\tilde{x}_l, \tilde{y}_l) & L_{22}(\tilde{x}_l, \tilde{y}_l) \end{pmatrix} \begin{pmatrix} x \\ y \end{pmatrix} := L(\tilde{x}_l, \tilde{y}_l) \begin{pmatrix} x \\ y \end{pmatrix},$$

where

$$(4.37) \quad L_{11}(\tilde{x}_l, \tilde{y}_l) = L_{22}(\tilde{x}_l, \tilde{y}_l) = -\frac{\lambda}{3} (\cos(\tilde{x}_l) \cosh(\tilde{y}_l) + 2 \cos(2\tilde{x}_l) \cosh(2\tilde{y}_l)),$$

$$(4.38) \quad -L_{21}(\tilde{x}_l, \tilde{y}_l) = L_{12}(\tilde{x}_l, \tilde{y}_l) = -\frac{\lambda}{3} (\sin(\tilde{x}_l) \sinh(\tilde{y}_l) + 2 \sin(2\tilde{x}_l) \sinh(2\tilde{y}_l)).$$

A straightforward calculation reveals that the eigenvalues  $\lambda_{l1}$  and  $\lambda_{l2}$  of the matrix  $L(\tilde{x}_l, \tilde{y}_l)$  have same real part:

$$(4.39) \quad \Re(\lambda_{l1}) = \Re(\lambda_{l2}) = -\frac{\lambda}{3} (\cos(\tilde{x}_l) \cosh(\tilde{y}_l) + 2 \cos(2\tilde{x}_l) \cosh(2\tilde{y}_l)).$$

We observe that by using the second equation of system equations (4.19), the real part of the eigenvalues may be written as

$$(4.40) \quad \Re(\lambda_{l1}) = \Re(\lambda_{l2}) = -\frac{\lambda}{3} \cos(\tilde{x}_l) \left( \cosh(\tilde{y}_l) - \frac{2 \sinh(\tilde{y}_l) \cosh(2\tilde{y}_l)}{\sinh(2\tilde{y}_l)} \right).$$

Since for all  $y > 0$ ,

$$\begin{aligned} & \cosh(y) - \frac{2 \sinh(y) \cosh(2y)}{\sinh(2y)} = \cosh(y) - \frac{\cosh(2y)}{\cosh(y)} = \frac{\cosh^2(y) - \cosh(2y)}{\cosh(y)} \\ & = \frac{\cosh^2(y) - (2 \cosh^2(y) - 1)}{\cosh(y)} = \frac{1 - \cosh^2(y)}{\cosh(y)} < 0, \end{aligned}$$

by checking the sign of  $\cos(\tilde{x}_l)$  we see that  $\Re(\lambda_{l1}) = \Re(\lambda_{l2}) > 0$  when  $l = 1$  and, on the other hand,  $\Re(\lambda_{l1}) = \Re(\lambda_{l2}) < 0$  when  $l = 3$ . Applying the Hartman–Grobman theorem, the claim we set out to prove is now verified. To recapitulate, we proved that in  $R_0$ , one of these equilibria is a stable equilibrium  $(\tilde{x}_3, \tilde{y}_3) := (x^0, y^0)$  and the other is an unstable equilibrium  $(\tilde{x}_1, \tilde{y}_1) := (\bar{x}^0, \bar{y}^0)$ . Finally, the periodicity let us conclude that, in  $R_k$ , there exists only one stable equilibrium  $(x^k, y^k)$  such that  $x^k \in (2k\pi + r_3, 2k\pi + 5\pi/4)$  and only one unstable equilibrium  $(\bar{x}^k, \bar{y}^k)$  such that  $\bar{x}^k \in (2k\pi + \pi/4, 2k\pi + r_1)$ .

**4.2.2. “Critically weak” and “weak” cases  $\Lambda_c \leq \lambda < \lambda_c = \omega$ .** First, we focus on the “critically weak” case  $\lambda = \Lambda_c$ . We claim that the system of equations (4.17) possesses two equilibria in  $R_k$  (recall (4.18)). Thus we may verify that one of the equilibrium points is  $(x, y) = (r_1, 0)$ ; see Fig. 6. This equilibrium is not stable, since the stable manifold  $W^s(r_1, 0)$  contains at least  $\{(x, y) : 0 < x \leq r_1, y = 0\}$  and on the other hand, the unstable manifold  $W^u(r_1, 0)$  contains at least  $\{(x, y) : r_1 < x < 2\pi, y = 0\}$ , which follows from the real Kuramoto model. That is, we verify the result of Cherry flow with the same natural frequency gaps in [29] (see Fig. 2(b) therein; our result recovers the stability of equilibria on the diagonal of that figure) when  $0.852\dots < \lambda/\omega < 1$ , and we characterize the exact lower bound as  $3/(2 \max_{x \in \mathbb{R}} (\sin(x) + \sin(2x))) = \sqrt{\frac{69-11\sqrt{33}}{8}} \approx 0.85218915$ , while the rough lower bound on  $\lambda/\omega$  given in [29] corresponds to  $1.70/2 = 0.85$ .

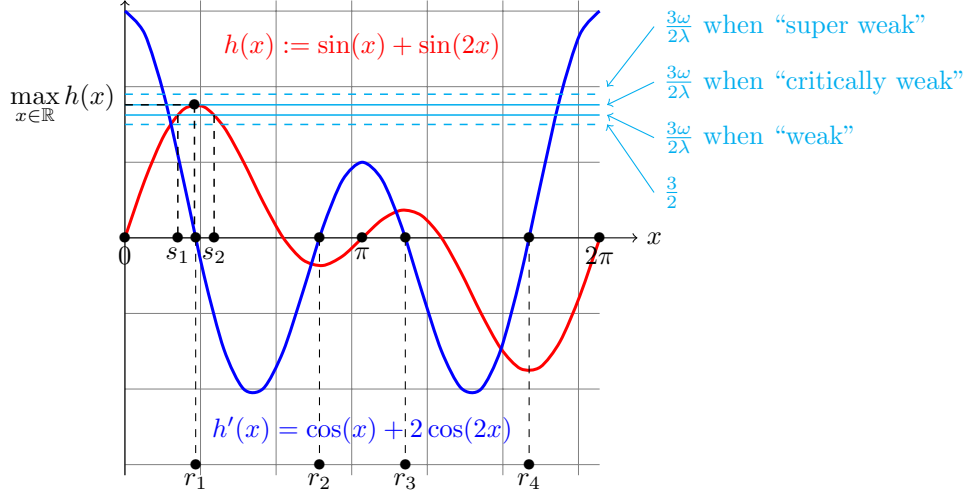


FIG. 6. This plot is an illustration of the function  $h(x)$  and its derivative  $h'(x)$  on the interval  $[0, 2\pi]$ . We also clarify the values of  $3\omega/(2\lambda)$  for “super weak”, “critically weak” and “weak” coupling in cyan: “super weak” when  $3\omega/(2\lambda) > \max_{x \in \mathbb{R}} h(x)$ , “critically weak” when  $3\omega/(2\lambda) = \max_{x \in \mathbb{R}} h(x)$ , and “weak” when  $3/2 < 3\omega/(2\lambda) < \max_{x \in \mathbb{R}} h(x)$ .

Following a similar argument from the super weak coupling and recalling the definition of  $f$ ,  $g_1$  and  $g_2$  in (4.26), (4.27) and (4.28), we notice that any equilibrium point with  $y > 0$  cannot exist in either  $x \in (\frac{3\pi}{4}, r_2) \cup (r_4, \frac{7\pi}{4})$  or  $(\frac{\pi}{4}, r_1)$ , since  $f(x, g_1^{-1}g_2(x)) < 0$  when  $x \in (\frac{\pi}{4}, r_1)$ .

This latter fact can be shown via a straightforward argument using calculus. First, we observe that  $\frac{d^2}{dx^2} f(x, g_1^{-1}g_2(x)) < 0$  when  $x \in (\frac{\pi}{4}, r_1)$  once the second derivative is calculated and simplified. This implies that the derivative  $\frac{d}{dx} f(x, g_1^{-1}g_2(x))$  is strictly decreasing. Since it can be readily computed that  $\frac{d}{dx} f(x, g_1^{-1}g_2(x))|_{x=r_1} > 0$ , this implies that  $\frac{d}{dx} f(x, g_1^{-1}g_2(x)) > 0$  on  $(\frac{\pi}{4}, r_1)$ . Then, observing that

$$f(x, g_1^{-1}g_2(x))|_{x=r_1} = f(r_1, 0) = \frac{3\omega}{2\lambda} - (\sin(r_1) + \sin(2r_1))$$

from (4.32) is not positive in the (critically) weak regime  $\Lambda_c \leq \lambda < \lambda_c$ , we conclude that  $f(x, g_1^{-1}g_2(x)) < 0$  when  $x \in (\frac{\pi}{4}, r_1)$ .

Using Lemma 4.5 and applying (4.34) and (4.35), we obtain that there is a second equilibrium point whose real part belongs to  $(r_3, \frac{5\pi}{4}) \subset (\pi, \frac{5\pi}{4})$ , on which cosine is negative. From (4.40) we then conclude that the equilibrium point is asymptotically stable.

Finally, we restrict our attention to the “weak” case. When  $\Lambda_c < \lambda < \lambda_c$ , the system equations (4.17) possesses three equilibria in  $R_k$  (recall (4.18)). We find that the first equilibrium point is a stable equilibrium, whose  $x$ -coordinate belongs to  $[r_3, \frac{5\pi}{4})$  and  $y$ -coordinate is strictly positive from (4.34), (4.35). Next, based on Fig. 6, we observe that the second and third equilibria are  $(x, y) = (s_1, 0)$  and  $(x, y) = (s_2, 0)$ , where  $s_1$  is the unique solution to  $h(x) = 3\omega/(2\lambda)$  with  $s_1 < r_1$ , and  $s_2$  is the unique solution to  $h(x) = 3\omega/(2\lambda)$  with  $s_2 > r_1$ . These two equilibrium points bifurcate from  $(r_1, 0)$  when  $\lambda$  exceeds the critically weak coupling strength  $\Lambda_c$ . However, since  $y = 0$ , linearization does not work as the real part of eigenvalues of the linearization

vanishes per (4.40). Therefore, the following Theorem 4.6 is formulated and proved using a different approach. A brief sketch of proof is as follows. A simple observation shows that  $(s_2, 0)$  is unstable. To prove that  $(s_1, 0)$  is stable, we need a more detailed characterization of the trajectory (see Fig. 7). We employ the implicit function theorem to identify an auxiliary function  $S : Y \rightarrow \mathbb{R}$  defined in the proof of Theorem 4.6. Given  $t > 0$ , using  $S(y(t))$ , we determine the sign of  $\dot{x}(t)$ . Finally, we can show that  $S(y(t))$  approaches  $s_1$  as  $t \rightarrow \infty$ , and use it to establish the following theorem.

**THEOREM 4.6.** *The equilibrium  $(s_1, 0)$  is asymptotically stable and the equilibrium  $(s_2, 0)$  is unstable.*

*Proof.* Let us first show that  $(s_2, 0)$  is unstable. Based on Fig. 6, we observe that  $\cos(s_2) + 2 \cos(2s_2) < 0$ . Recalling the second equation in (4.17), we have

$$\dot{y} = -\frac{\lambda}{3} (\cos(x) + 2 \cos(2x) \cosh(y)) \sinh(y).$$

One may observe that there exists a sufficiently small  $\epsilon > 0$  such that

$$\begin{cases} \dot{y} < 0 & \text{when } |x - s_2| < \epsilon \text{ and } -\epsilon < y < 0, \\ \dot{y} > 0 & \text{when } |x - s_2| < \epsilon \text{ and } 0 < y < \epsilon. \end{cases}$$

Therefore,  $(s_2, 0)$  is an unstable equilibrium.

Second, let us show that  $(s_1, 0)$  is asymptotically stable. Let us consider the case where the initial condition is on the real line. By uniqueness, (4.17) reduces to

$$\dot{x} = \frac{\omega}{2} - \frac{\lambda}{3} (\sin(x) + \sin(2x)).$$

Based on Fig. 6, there exists  $\delta > 0$  such that

$$\begin{cases} \dot{x} > 0 & \text{when } s_1 - \delta < x < s_1, \\ \dot{x} < 0 & \text{when } s_1 < x < s_1 + \delta. \end{cases}$$

Therefore, given an initial condition  $(x(0), y(0))$  satisfying  $|x(0) - s_1| < \delta$  and  $y(0) = 0$ , we obtain

$$\lim_{t \rightarrow \infty} (x(t), y(t)) = (s_1, 0).$$

Recall (4.26) and Fig. 6, one may observe that  $f(s_1, 0) = 0$  and  $(\partial f / \partial x)(s_1, 0) < 0$ . By implicit function theorem, there exists an open set  $Y \subset \mathbb{R}$  containing 0, and a unique function  $S : Y \rightarrow \mathbb{R}$  such that  $S(0) = s_1$ , and  $f(S(y), y) = 0$  for all  $y \in Y$ . By the evenness of  $\cosh(\cdot)$ , from (4.26) we see that  $S(\cdot)$  is an even function. Moreover,  $S$  is continuously differentiable and  $S' < 0$  in  $Y \cap \{y > 0\}$  and  $S' > 0$  in  $Y \cap \{y < 0\}$  by choosing small enough domain  $Y$ .

Next, let us define  $\delta := h'(s_1)/2 = (\cos(s_1) + 2 \cos(2s_1))/2 > 0$  (see Fig. 6) and then choose a sufficiently small  $\epsilon > 0$  such that  $(-\epsilon, \epsilon) \subset Y$ ,

$$(4.41) \quad \begin{cases} \dot{y} > 0 & \text{when } S(\epsilon) < x < 2s_1 - S(\epsilon) \text{ and } -\epsilon < y < 0, \\ \dot{y} < 0 & \text{when } S(\epsilon) < x < 2s_1 - S(\epsilon) \text{ and } 0 < y < \epsilon, \end{cases}$$

$$(4.42) \quad \frac{\omega}{2} - \frac{\lambda}{3} (\sin(S(\epsilon)) \cosh(\epsilon) + \sin(2S(\epsilon)) \cosh(2\epsilon)) = 0,$$

$$(4.43) \quad \frac{\partial f}{\partial x}(x, y) < 0 \text{ when } S(\epsilon) < x < 2s_1 - S(\epsilon) \text{ and } -\epsilon < y < \epsilon,$$

$$(4.44) \quad \cos(x) + 2 \cos(2x) \cosh(y) > \delta \text{ when } S(\epsilon) < x < 2s_1 - S(\epsilon) \text{ and } -\epsilon < y < \epsilon,$$

$$0 < S(\epsilon) < s_1 \text{ and } 2s_1 - S(\epsilon) < r_1.$$

We observe that, for all  $|y_1| < |y_2| < \epsilon$ ,

$$(4.45) \quad 0 < S(\epsilon) < S(y_2) < S(y_1) < s_1,$$

and

$$(4.46) \quad \lim_{y_1 \rightarrow 0} S(y_1) = s_1.$$

Let

$$(4.47) \quad \begin{aligned} B^+(\epsilon) &:= \left\{ (x, y) \mid S(\epsilon) < x < 2s_1 - S(\epsilon) \text{ and } 0 < y < \epsilon \right\}, \\ B^-(\epsilon) &:= \left\{ (x, y) \mid S(\epsilon) < x < 2s_1 - S(\epsilon) \text{ and } -\epsilon < y < 0 \right\}. \end{aligned}$$

Given an initial condition  $(x(0), y(0)) \in B^+(\epsilon)$ , we first show that

$$(4.48) \quad (x(t), y(t)) \in B^+(\epsilon) \text{ for } t > 0.$$

Suppose (4.48) does not hold. There exists the first moment  $t_0 > 0$  such that  $(x(t_0), y(t_0))$  hits the boundary of the box  $B^+(\epsilon)$ . Due to (4.41), we have  $y(0) > y(t_0)$ , which ensures that  $y$  cannot reach the upper boundary  $y = \epsilon$  at the moment  $t_0$ . Also, the uniqueness of the solution ensures that  $y$  cannot reach the lower boundary  $y = 0$ . In other words, the first time  $(x(t), y(t))$  reaches the boundary implies that either  $x(t_0) = 2s_1 - S(\epsilon)$  or  $x(t_0) = S(\epsilon)$ . Moreover, since hitting the upper and lower boundary is impossible, we can further conclude that  $S(\epsilon) < x(t) < 2s_1 - S(\epsilon)$  for all  $0 < t < t_0$ . Then we consider the following two cases.

*Case 1.*  $x(t_0) = 2s_1 - S(\epsilon)$ . It is clear from first hitting that  $\dot{x}(t_0) \geq 0$ . On the other hand, recalling (4.17), we see that

$$\begin{aligned} \dot{x}(t_0) &= \frac{\omega}{2} - \frac{\lambda}{3} (\sin(x(t_0)) \cosh(y(t_0)) + \sin(2x(t_0)) \cosh(2y(t_0))) \\ &\leq \frac{\omega}{2} - \frac{\lambda}{3} (\sin(x(t_0)) + \sin(2x(t_0))) \\ &= \frac{\omega}{2} - \frac{\lambda}{3} (\sin(2s_1 - S(\epsilon)) + \sin(2(2s_1 - S(\epsilon)))) \stackrel{\text{Fig. 6}}{<} 0, \end{aligned}$$

which leads to a contradiction.

*Case 2.*  $x(t_0) = S(\epsilon)$ . It is clear from first hitting that  $\dot{x}(t_0) \leq 0$ . On the other hand, recalling (4.17) again, we see that

$$(4.49) \quad \begin{aligned} \dot{x}(t_0) &= \frac{\omega}{2} - \frac{\lambda}{3} (\sin(x(t_0)) \cosh(y(t_0)) + \sin(2x(t_0)) \cosh(2y(t_0))) \\ &> \frac{\omega}{2} - \frac{\lambda}{3} (\sin(S(y(t_0))) \cosh(y(t_0)) + \sin(2S(y(t_0))) \cosh(2y(t_0))) \stackrel{(4.42)}{=} 0, \end{aligned}$$



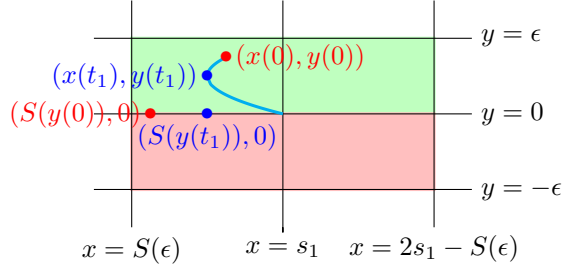


FIG. 7. The plot shows the  $B^+(\epsilon)$  (green region) and  $B^-(\epsilon)$  (red region) defined in (4.47). The cyan trajectory with initial condition  $(x(0), y(0))$  is the solution of (4.17). The smooth function  $S$  is defined in the proof of Theorem 4.6.

where the inequality comes from the fact that  $y(t_0) < \epsilon \implies S(y(t_0)) > S(\epsilon) = x(t_0)$  and (4.43). So in this case, we also arrive at a contradiction. Hence, by *Case 1.* and *Case 2.*, (4.48) is shown. Combining this with (4.41), we know  $y(t)$  is always positive and decreases to zero (since if the limit  $\bar{y} > 0$ , then applying (4.44) in the second equation of (4.17) gives  $\dot{y} < -\lambda\delta \sinh(\bar{y})/3$ , giving a contradiction). Therefore,  $S(y(t))$  tends to  $s_1$  as  $t$  tends to infinity.

Finally, we show that

$$(4.50) \quad \lim_{t \rightarrow \infty} (x(t), y(t)) = (s_1, 0).$$

for initial conditions  $(x(0), y(0)) \in B^+(\epsilon)$ .

Given  $0 < \epsilon_1 < \epsilon$ , there exists a  $T > 0$  such that  $0 < y(T) < \epsilon_1$  and  $0 < s_1 - S(y(T)) < \epsilon_1$ . If  $x(T) = S(y(T))$ , following a similar argument as (4.48), we are done. Otherwise, we consider the following two cases for  $x(T)$ .

*Case I.*  $x(T) < S(y(T))$ . First, suppose  $x(t) < S(y(t))$  for  $t > T$ . Following the same argument as (4.49), we have  $\dot{x}(t) > 0$  for  $t > T$ . Combining with (4.45) and (4.46), we see that  $x(t)$  is increasing and bounded by  $s_1$ , hence  $\lim_{t \rightarrow \infty} x(t) = \bar{x}$  exists.

Moreover, one can show  $\bar{x} = s_1$  through a contradiction argument using (4.49). On the other hand, if there exists a  $T_0 > T$  such that  $x(T_0) = S(y(T_0))$ , following a similar argument as (4.48), we know  $(x(t), y(t)) \in B^+(\epsilon_1)$  for  $t > T_0$ .

*Case II.*  $x(T) > S(y(T))$ . First, suppose  $x(t) > S(y(t))$  for  $t > T$ . Then similarly to *Case I.*, we have  $\dot{x}(t) < 0$  for  $t > T$ . Combining with (4.45) and (4.46), we notice that  $|x(t) - S(y(t))|$  is decreasing for  $t > T$ . Moreover,  $x(T) > s_1$  (otherwise we have the case  $x(T_0) = S(y(T_0))$  below), and following a similar argument as *Case I.* we have  $\lim_{t \rightarrow \infty} x(t) = s_1$ . On the other hand, if there exists a  $T_0 > T$  such that  $x(T_0) = S(y(T_0))$ , following a similar argument as (4.48), we know  $(x(t), y(t)) \in B^+(\epsilon_1)$  for  $t > T_0$ .

Hence, by *Case I.* and *Case II.*, we can find a sequence of the boxes  $\{B^+(\epsilon_j)\}$  such that  $B^+(\epsilon) \supset B^+(\epsilon_1) \supset B^+(\epsilon_2) \supset \dots$  as  $\epsilon > \epsilon_1 > \epsilon_2 > \dots$  and  $\lim_{j \rightarrow \infty} \epsilon_j = 0$ , so (4.50) is complete. One may similarly show that  $\lim_{t \rightarrow \infty} (x(t), y(t)) = (s_1, 0)$  for initial conditions  $(x(0), y(0)) \in B^-(\epsilon)$ . This completes the proof of Theorem 4.6.  $\square$

**4.2.3. Numerical Results.** We conduct brief numerical simulations, the results of which are presented in Fig. 8, to verify our theorems in the previous subsections of Sec. 4.2. In particular, based on the equivalent ODE system (4.17) derived from applying the *Cherry flow*-like ansatz in the  $N = 3$  complexified Kuramoto systems (2.2), we numerically evaluate its flow fields (also called slope fields) under different regimes

of weak coupling. In all three sub-figures in Fig. 8, the horizontal axis represents the  $x$  variable, while the vertical axis represents  $y$ . By periodicity of the system (4.17) in the  $x$  variable, we only plot the flow fields over the horizontal range  $x \in [0, 2\pi]$ ; for the purpose of illustration we choose to only plot over the vertical range  $y \in [-2, 2]$ .

The system parameters of this numerical evaluation are listed below. We choose the maximum frequency gap  $\omega = 1$ . In Fig. 8a, we choose  $\lambda = 0.7$ , which falls in the “super weak” coupling regime; in Fig. 8b, we choose  $\lambda = \sqrt{(69 - 11\sqrt{33})}/8 = 0.85218915\dots$ , which corresponds to the “critically weak” coupling case; and in Fig. 8c, we choose  $\lambda = 0.99$ , which falls in the “weak” coupling regime.

The figures are consistent with our theorems in the previous subsections of Sec. 4.2. First, in Fig. 8a we observe that there are indeed two complex equilibria in  $R_0$  (see (4.18)). With reference to subsection 4.2.1, we verify that the left one is unstable (i.e.,  $(\bar{x}^0, \bar{y}^0)$ ) while the right one is stable (i.e.,  $(x^0, y^0)$ ). Second, in Fig. 8b we observe two equilibria in  $R_0$ , one real and the other complex. With reference to subsection 4.2.2, we verify that the left one is unstable (i.e.,  $(r_1, 0)$ ) while the right one is stable. Finally, in Fig. 8c we observe three equilibria in  $R_0$ , two real and the other complex. With reference to subsection 4.2.2 and Theorem 4.6, we verify that the left real one is stable (i.e.,  $(s_1, 0)$ ), the right real one is unstable (i.e.,  $(s_2, 0)$ ), while the complex one is stable.

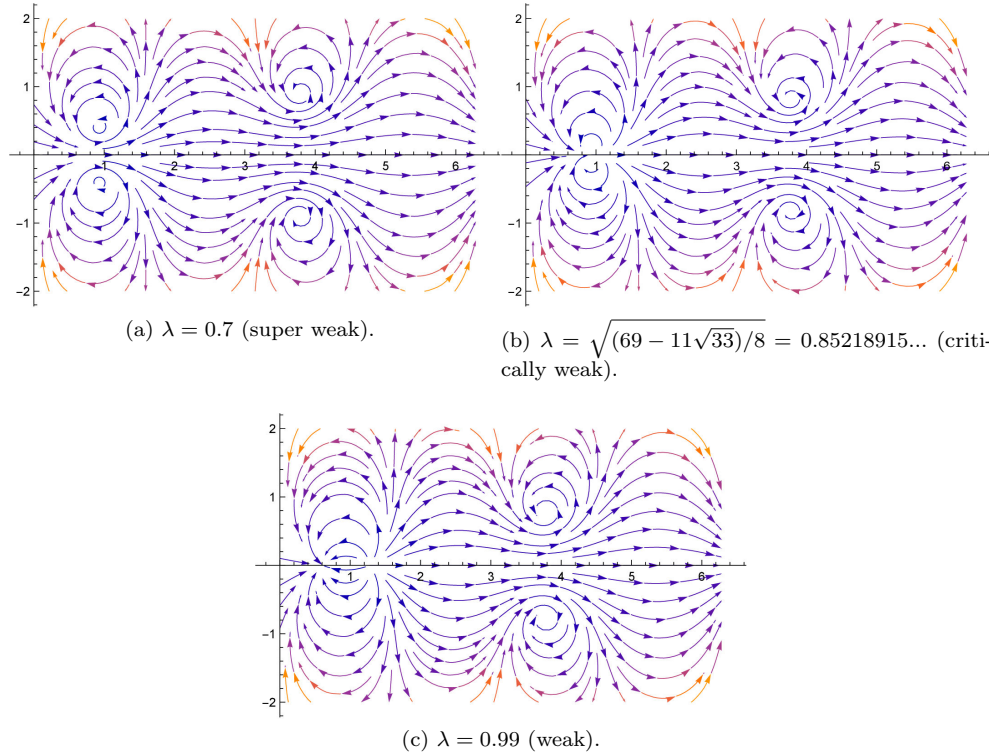


FIG. 8. Example flow fields of the equivalent system (4.17) of  $N = 3$  oscillators under the Cherry flow-like ansatz. Here, we choose  $\omega = 1$ . The horizontal axis represents the  $x$  variable, and the vertical axis represents the  $y$  variable.

**5. Acknowledgement.** We express our gratitude for the insightful discussions generously provided by Zih-Hao Huang and Yen-Ting Lin.

**6. Data Availability Statement.** Data will be made available on reasonable request.

**7. Declaration.** We do not have any conflict of interest.

**8. Appendix.**

**8.1. Proof of  $\delta/n$  criterion.** Define

$$(8.1) \quad \tilde{Q}_{2k} := Q_{2k} \cap \left\{ (x, y) \mid \omega - \lambda \sin(x) \cosh(y) \geq 0, x \geq x(0) \right\}.$$

We illuminate this in Fig. 3, where the cyan curve represents  $\omega - \lambda \sin(x) \cosh(y) = 0$ . We observe that the solution  $(x(t), y(t))$  with the initial condition (4.6) keeps staying at the right-hand side of the vertical line  $x = x(0)$ , since  $\dot{x} \geq 0$ . Also, the solution cannot cross the cyan curve  $\omega - \lambda \sin(x) \cosh(y) = 0$ , since  $\dot{x} = 0$  and  $\dot{y} < 0$ . If the conclusion (4.7) is not true, then the solution  $(x(t), y(t))$  will stay at the region  $\tilde{Q}_{2k}$  for any finite time  $t > 0$ . By Poincaré–Bendixson theorem, this implies the trajectory satisfies

$$(8.2) \quad (x(t), y(t)) \in \tilde{Q}_{2k} \text{ when } 0 < t < \infty,$$

and

$$(8.3) \quad \lim_{t \rightarrow \infty} (x(t), y(t)) = (x_k, \alpha).$$

On the other hand, consider a  $\delta > 0$ , such that  $x(0) + \delta < x_k$ . Let  $P_n = (\varpi_0, \varpi_1, \dots, \varpi_n)$  be a partition of the closed interval  $[x(0), x(0) + \delta]$  and  $\varpi_l = x(0) + l\delta/n$  for each  $l \in \{0, 1, \dots, n\}$ . Our goal here is to construct an infinite-layer “ $\delta/n$  buffer” to slow down the solution and avoid it approaching the equilibrium point  $(x_k, \alpha)$ . In the region  $\tilde{Q}_{2k} \cap \{\varpi_{l-1} < x < \varpi_l\}$ , for  $l = 1, \dots, n$ , we notice that

$$(8.4) \quad \dot{x} = \omega - \lambda \sin(x) \cosh(y) \leq \omega - \lambda \sin(\varpi_{l-1}) \cosh(\alpha),$$

and

$$(8.5) \quad |\dot{y}| = \lambda \cos(x) \sinh(y) \geq \lambda \cos(\varpi_l) \sinh(\alpha).$$

Because of (8.2) and (8.3), there exists a  $\tilde{t}$  such that  $x(\tilde{t}) = \varpi_n$  and  $y(\tilde{t}) > \alpha$ . Also, we obtain

$$(8.6) \quad y_0 - \alpha > \int_0^{\tilde{t}} -\dot{y} dt = \int_{x(0)}^{x(\tilde{t})} -\frac{\dot{y}}{\dot{x}} dx = \sum_{l=0}^n \int_{\varpi_l}^{\varpi_{l+1}} -\frac{\dot{y}}{\dot{x}} dx.$$

By means of (8.4) and (8.5), we arrive at

$$\begin{aligned}
& \sum_{l=0}^n \int_{\varpi_l}^{\varpi_{l+1}} -\frac{\dot{y}}{\dot{x}} dx \\
& \geq \sum_{l=0}^n \frac{\lambda \cos(\varpi_l) \sinh(\alpha)}{\omega - \lambda \sin(\varpi_{l-1}) \cosh(\alpha)} \cdot \frac{\delta}{n} = \tanh(\alpha) \sum_{l=0}^n \frac{\cos(\varpi_l)}{1 - \sin(\varpi_{l-1})} \cdot \frac{\delta}{n} \\
& = \tanh(\alpha) \left( \cos\left(\frac{\delta}{n}\right) \sum_{l=0}^n \frac{\cos(\varpi_{l-1})}{1 - \sin(\varpi_{l-1})} \cdot \frac{\delta}{n} \right. \\
(8.7) \quad & \left. - \sin\left(\frac{\delta}{n}\right) \sum_{l=0}^n \frac{\sin(\varpi_{l-1})}{1 - \sin(\varpi_{l-1})} \cdot \frac{\delta}{n} \right).
\end{aligned}$$

We notice that inequality (8.7) holds for all  $n \in \mathbb{N}$ . Therefore, combining (8.6) and (8.7) results in

$$\begin{aligned}
& y_0 - \alpha \\
& \geq \tanh(\alpha) \cdot \lim_{n \rightarrow \infty} \left\{ \cos\left(\frac{\delta}{n}\right) \sum_{l=0}^n \frac{\cos(\varpi_{l-1})}{1 - \sin(\varpi_{l-1})} \cdot \frac{\delta}{n} \right. \\
& \quad \left. - \sin\left(\frac{\delta}{n}\right) \sum_{l=0}^n \frac{\sin(\varpi_{l-1})}{1 - \sin(\varpi_{l-1})} \cdot \frac{\delta}{n} \right\} \\
& = \tanh(\alpha) \cdot \int_{x(0)}^{x(0)+\delta} \frac{\cos(x)}{1 - \sin(x)} dx = \tanh(\alpha) \cdot \ln\left(\frac{1 - \sin(x(0))}{1 - \sin(x(0) + \delta)}\right),
\end{aligned}$$

which is bounded. This is a contradiction of

$$(8.8) \quad \ln\left(\frac{1 - \sin(x(0))}{1 - \sin(x(0) + \delta)}\right) \rightarrow \infty,$$

as  $\delta \rightarrow x_k - x(0)$ . This contradiction thus asserts that there exists a finite time  $T > 0$  such that

$$(8.9) \quad (x(T), y(T)) \in \left\{ (x, y) \mid x_k - \frac{\pi}{2} < x < x_k, y = \alpha \right\}.$$

## 8.2. Proof of symmetric property. Let

$$(8.10) \quad \mathbf{x}(t) := 2x_k - x(T - t),$$

$$(8.11) \quad \mathbf{y}(t) := y(T - t),$$

for  $0 \leq t \leq T$ . Notice that  $\mathbf{x}(0) = x_k = x(T)$  and  $\mathbf{y}(0) = y(T)$ . Also,

$$\begin{aligned}
\dot{\mathbf{x}}(t) &= \dot{x}(T - t) = \omega - \lambda \sin(x(T - t)) \cosh(y(T - t)) \\
&= \omega - \lambda \sin(\mathbf{x}(t)) \cosh(\mathbf{y}(t)); \\
\dot{\mathbf{y}}(t) &= -\dot{y}(T - t) = \lambda \cos(x(T - t)) \sinh(y(T - t)) \\
&= -\lambda \cos(\mathbf{x}(t)) \sinh(\mathbf{y}(t)),
\end{aligned}$$

such that  $(\mathbf{x}(t), \mathbf{y}(t))$  also satisfies the original system equations (4.1).

Through the existence and uniqueness of the solution, we have

$$\begin{aligned}\mathbf{x}(t) &= x(t+T), \\ \mathbf{y}(t) &= y(t+T),\end{aligned}$$

for  $t \in [0, T]$ . We pause to remark that the dynamical system must continually evolve until at least  $t = 2T$ . Otherwise, if there is a  $t_0 \in (T, 2T)$  such that  $x$  or  $y$  goes to infinity by symmetry up to  $t_0 - \epsilon$ , there is a contradiction through the continuity argument. Combining (8.10) and (8.11) implies that

$$\begin{aligned}x(T-t) + x(T+t) &= 2x_k, \\ y(T-t) - y(T+t) &= 0,\end{aligned}$$

so the solution must be symmetric with respect to the vertical line  $x = x_k$ .

### 8.3. Proof of deceleration/acceleration region.

*Proof.* Recall that  $x_k = \frac{\pi}{2} + 2k\pi$ . Since both the function  $F_k$  and the sets  $S_k^-$ ,  $S_k^+$  are periodic  $2\pi$ , it suffices to focus on the case  $k = 0$ . For brevity, we write  $F := F_0$ .

To determine the sign of  $F$ , we argue through the signs of its partial derivatives  $F_x$  and  $F_{xx}$ . A summary of the signs of  $F$ ,  $F_x$  and  $F_{xx}$  are given in Fig. 9.

First, we check that, for all  $y$ ,

$$\begin{aligned}F(0, y) &= -\frac{\pi}{2}\gamma - (y - \alpha)\sinh(y), \\ F\left(\frac{\pi}{2}, y\right) &= 0, \\ F(\pi, y) &= \frac{\pi}{2}\gamma + (y - \alpha)\sinh(y).\end{aligned}$$

Since the function  $h_1(y) := (y - \alpha)\sinh(y)$  is continuous and  $h_1(\alpha) = 0$ , there exists an  $\epsilon_1 > 0$  such that for all  $(1 - \epsilon_1)\alpha < y < (1 + \epsilon_1)\alpha$ , we have  $|h_1(y)| < \pi\gamma/2$ . Therefore, whenever  $(1 - \epsilon_1)\alpha < y < (1 + \epsilon_1)\alpha$ , we have  $F(0, y) < 0$  and  $F(\pi, y) > 0$ .

Second, we look at the partial derivative  $F_x$ . A straightforward calculation yields that

$$\begin{aligned}F_x(x, y) &:= \frac{\partial}{\partial x}F(x, y) \\ &= \gamma - \sin(x)\cosh(y) \\ &\quad - \left(x - \frac{\pi}{2}\right)\cos(x)\cosh(y) + (y - \alpha)\sin(x)\sinh(y).\end{aligned}$$

Hence, we have

$$\begin{aligned}F_x(0, y) &= F_x(\pi, y) = \gamma + \frac{\pi}{2}\cosh(y) \geq \gamma + \frac{\pi}{2} > 0, \\ F_x\left(\frac{\pi}{2}, y\right) &= \gamma - \cosh(y) + (y - \alpha)\sinh(y).\end{aligned}$$

We notice that  $F_x(\pi/2, \alpha) = 0$ . To determine the sign of  $F_x(\pi/2, y)$  for  $y$  close to  $\alpha$ , we consider the derivative of  $F_x(\pi/2, y)$  w.r.t.  $y$ . Equivalently,

$$F_{xy}\left(\frac{\pi}{2}, y\right) := \frac{\partial^2}{\partial y \partial x}F(x, y) \Big|_{x=\frac{\pi}{2}} = (y - \alpha)\cosh(y).$$

It is now clear that  $F_{xy}(\pi/2, y) < 0$  when  $y < \alpha$  and that  $F_{xy}(\pi/2, y) > 0$  when  $y > \alpha$ . Hence,  $F_x(\pi/2, y)$  is minimized at and only at  $y = \alpha$ . That is,

$$F_x\left(\frac{\pi}{2}, y\right) \geq F_x\left(\frac{\pi}{2}, \alpha\right) = 0.$$

Third, we look at the second-order partial derivative  $F_{xx}$ . A straightforward calculation results in

$$\begin{aligned} F_{xx}(x, y) &:= \frac{\partial^2}{\partial x^2} F(x, y) \\ &= -2 \cos(x) \cosh(y) \\ (8.12) \quad &+ \left(x - \frac{\pi}{2}\right) \sin(x) \cosh(y) + (y - \alpha) \cos(x) \sinh(y) \\ &= -\cos(x) \cdot (2 \cosh(y) - (y - \alpha) \sinh(y)) \\ &- \left(\frac{\pi}{2} - x\right) \sin(x) \cosh(y). \end{aligned}$$

Let us first restrict  $x$  to be in the open interval  $(0, \pi/2)$ . Then,  $\cos(x) > 0$ ,  $\pi/2 - x > 0$ ,  $\sin(x) > 0$  and  $\cosh(y) > 0$ , so as long as  $y$  allows the function  $h_2(y) := 2 \cosh(y) - (y - \alpha) \sinh(y)$  to be positive, then from (8.12) we have  $F_{xx} < 0$ . Since  $h_2(\alpha) = 2\gamma > 0$ , by continuity of  $h_2$ , there exists an  $\epsilon_2 > 0$  such that  $h_2(y) > 0$  for all  $(1 - \epsilon_2)\alpha < y < (1 + \epsilon_2)\alpha$ .

Now, let us restrict  $x$  to be in the open interval  $(\pi/2, \pi)$ . Then,  $\cos(x) < 0$ ,  $\pi/2 - x < 0$ ,  $\sin(x) > 0$  and  $\cosh(y) > 0$ , so as long as  $y$  allows  $h_2(y)$  to be positive, from (8.12) we have  $F_{xx} > 0$ . Thus the same  $\epsilon_2$  works.

Let  $\epsilon = \min\{\epsilon_1, \epsilon_2\}$ . Define two sets in the  $(x, y)$ -plane around the equilibrium point  $(\pi/2, \alpha)$ :

$$\begin{aligned} S_0^- &:= \left\{ (x, y) \mid 0 < x < \frac{\pi}{2}, (1 - \epsilon)\alpha < y < (1 + \epsilon)\alpha \right\}; \\ S_0^+ &:= \left\{ (x, y) \mid \frac{\pi}{2} < x < \pi, (1 - \epsilon)\alpha < y < (1 + \epsilon)\alpha \right\}. \end{aligned}$$

For reasons that will become clear in the following argument, we shall call  $S_0^-$  the “deceleration region” and  $S_0^+$  the “acceleration region” for convenience. We illuminate this in Fig. 9, where the “deceleration region” is the red region, and the “acceleration region” is the green region.

Fix any  $y \in ((1 - \epsilon)\alpha, (1 + \epsilon)\alpha)$ , which defines a horizontal slice through the two regions. Since  $F_{xx} < 0$  on  $S_0^-$ , the one-variable function  $F_x(x, y)$  is strictly decreasing. Because  $F_x(0, y) > 0$  and  $F_x(\pi/2, y) \geq 0$ , we must have

$$F_x(x, y) > 0 \text{ for } x \in \left(0, \frac{\pi}{2}\right).$$

That is, the one-variable function  $F(x, y)$  is strictly increasing. Since  $F(0, y) < 0$  and  $F(\pi/2, y) = 0$ , we then have

$$F(x, y) < 0 \text{ for } x \in \left(0, \frac{\pi}{2}\right).$$

Since  $y$  was arbitrarily chosen in  $((1 - \epsilon)\alpha, (1 + \epsilon)\alpha)$ , we obtain that

$$F(x, y) < 0 \text{ on } S_0^-.$$

An analogous argument lets us conclude that

$$F(x, y) > 0 \text{ on } S_0^+.$$

□

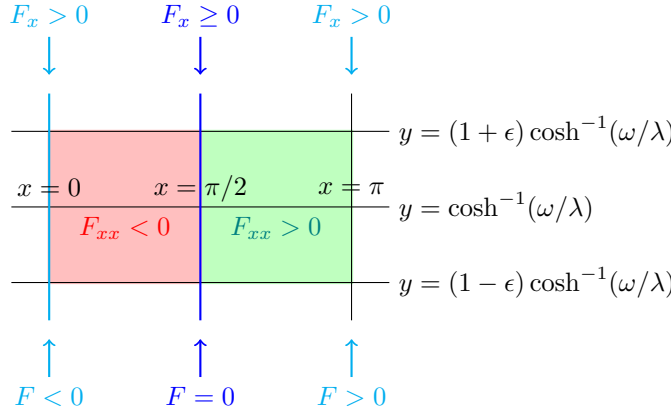


FIG. 9. This plot shows the “deceleration strip” (red) and “acceleration strip” (green) of the Lyapunov function  $L$  in a neighborhood of the equilibrium point  $(\pi/2, \cosh^{-1}(\omega/\lambda))$ .

#### REFERENCES

- [1] L. BASNARKOV AND V. URUMOV, *Phase transitions in the Kuramoto model*, Physical Review E, 76 (2007), p. 057201.
- [2] S. BOCCALETTI, J. KURTHS, G. OSIPOV, D. VALLADARES, AND C. ZHOU, *The synchronization of chaotic systems*, Physics Reports, 366 (2002), pp. 1–101.
- [3] L. BÖTTCHER AND M. A. PORTER, *Complex networks with complex weights*, Phys. Rev. E, 109 (2024), p. 024314.
- [4] J. C. BRONSKI, T. E. CARTY, AND L. DEVILLE, *Synchronisation conditions in the Kuramoto model and their relationship to seminorms*, Nonlinearity, 34 (2021), p. 5399.
- [5] J. C. BRONSKI, L. DEVILLE, AND M. JIP PARK, *Fully synchronous solutions and the synchronization phase transition for the finite- $N$  Kuramoto model*, Chaos: An Interdisciplinary Journal of Nonlinear Science, 22 (2012), p. 033133.
- [6] R. C. BUDZINSKI, T. T. NGUYEN, J. DOÀN, J. MINÁČ, T. J. SEJNOWSKI, AND L. E. MULLER, *Geometry unites synchrony, chimeras, and waves in nonlinear oscillator networks*, Chaos: An Interdisciplinary Journal of Nonlinear Science, 32 (2022), p. 031104.
- [7] R. C. BUDZINSKI, T. T. NGUYEN, J. DOÀN, J. MINÁČ, T. J. SEJNOWSKI, AND L. E. MULLER, *Analytical prediction of specific spatiotemporal patterns in nonlinear oscillator networks with distance-dependent time delays*, Phys. Rev. Res., 5 (2023), p. 013159.
- [8] R. CESTNIK AND E. A. MARTENS, *Integrability of a globally coupled complex Riccati array: Quadratic integrate-and-fire neurons, phase oscillators, and all in between*, Phys. Rev. Lett., 132 (2024), p. 057201.
- [9] S.-H. CHEN, C.-C. CHU, C.-H. HSIA, AND S. MOON, *Frequency synchronization of heterogeneous second-order forced Kuramoto oscillator networks: A differential inequality approach*, IEEE Transactions on Control of Network Systems, 10 (2023), pp. 530–543.
- [10] S.-H. CHEN, C.-C. CHU, C.-H. HSIA, AND M.-C. SHIUE, *Synchronization of heterogeneous forced first-order Kuramoto oscillator networks: A differential inequality approach*, IEEE Transactions on Circuits and Systems I: Regular Papers, 69 (2022), pp. 757–770.
- [11] S.-H. CHEN, C.-H. HSIA, AND M.-C. SHIUE, *On mathematical analysis of synchronization to bidirectionally coupled Kuramoto oscillators*, Nonlinear Analysis: Real World Applications, 56 (2020), p. 103169.
- [12] S.-H. CHOI AND S.-Y. HA, *Complete entrainment of Lohe oscillators under attractive and repulsive couplings*, SIAM Journal on Applied Dynamical Systems, 13 (2014), pp. 1417–1441.

- [13] L. DEVILLE, *Synchronization and Stability for Quantum Kuramoto*, Journal of Statistical Physics, 174 (2019), pp. 160–189.
- [14] F. DÖRFLER AND F. BULLO, *On the critical coupling for Kuramoto oscillators*, SIAM Journal on Applied Dynamical Systems, 10 (2011), pp. 1070–1099.
- [15] F. DÖRFLER AND F. BULLO, *Synchronization and transient stability in power networks and nonuniform Kuramoto oscillators*, SIAM Journal on Control and Optimization, 50 (2012), pp. 1616–1642.
- [16] F. DÖRFLER AND F. BULLO, *Synchronization in complex networks of phase oscillators: A survey*, Automatica, 50 (2014), pp. 1539–1564.
- [17] S.-Y. HA, M. KANG, AND B. MOON, *Collective behaviors of a Winfree ensemble on an infinite cylinder*, Discrete & Continuous Dynamical Systems-Series B, 26 (2021).
- [18] S.-Y. HA, M.-J. KANG, C. LATTANZIO, AND B. RUBINO, *A class of interacting particle systems on the infinite cylinder with flocking phenomena*, Mathematical Models and Methods in Applied Sciences, 22 (2012), p. 1250008.
- [19] S.-Y. HA, D. KO, J. PARK, AND X. ZHANG, *Collective synchronization of classical and quantum oscillators*, EMS Surv. Math Sci, 3 (2016), pp. 209–267.
- [20] S.-Y. HA, D. KO, AND S.-Y. RYOO, *On the relaxation dynamics of Lohe oscillators on some Riemannian manifolds*, Journal of Statistical Physics, 172 (2018), pp. 1427–1478.
- [21] S.-Y. HA AND S. RYOO, *Asymptotic phase-locking dynamics and critical coupling strength for the Kuramoto model*, Commun. Math Phys., 377 (2020), pp. 811–857.
- [22] C.-H. HSIA, C.-Y. JUNG, AND B. KWON, *On the synchronization theory of Kuramoto oscillators under the effect of inertia*, Journal of Differential Equations, 267 (2019), pp. 742–775.
- [23] C. HUYGENS AND R. BLACKWELL, *Christiaan Huygens' the Pendulum Clock, Or, Geometrical Demonstrations Concerning the Motion of Pendula as Applied to Clocks*, History of Science and Technology Series, Iowa State University Press, 1986.
- [24] A. JADBABAIE, N. MOTEE, AND M. BARAHONA, *On the stability of the Kuramoto model of coupled nonlinear oscillators*, in Proceedings of the 2004 American Control Conference, vol. 5, 2004, pp. 4296–4301.
- [25] Y. KURAMOTO, *Self-entrainment of a population of coupled non-linear oscillators*, in International Symposium on Mathematical Problems in Theoretical Physics, H. Araki, ed., Berlin, Heidelberg, Germany, 1975, Springer Berlin Heidelberg, pp. 420–422.
- [26] Y. KURAMOTO, *Chemical Oscillations, Waves, and Turbulence*, Springer Berlin, Heidelberg, Berlin, Heidelberg, Germany, 1984.
- [27] S. LEE, L. BRAUN, F. BÖNISCH, M. SCHRÖDER, M. THÜMLER, AND M. TIMME, *Complexified synchrony*, Chaos: An Interdisciplinary Journal of Nonlinear Science, 34 (2024), p. 053141.
- [28] M. A. LOHE, *Non-Abelian Kuramoto models and synchronization*, Journal of Physics A: Mathematical and Theoretical, 42 (2009), p. 395101.
- [29] Y. MAISTRENKO, O. POPOVYCH, O. BURLKO, AND P. A. TASS, *Mechanism of desynchronization in the finite-dimensional Kuramoto model*, Physical Review Letters, 93 (2004), p. 084102.
- [30] G. OSIPOV, J. KURTHS, AND C. ZHOU, *Synchronization in Oscillatory Networks*, Springer-Verlag Berlin, Berlin, Heidelberg, Germany, 2007.
- [31] D. PAZÓ, *Thermodynamic limit of the first-order phase transition in the Kuramoto model*, Physical Review E, 72 (2005), p. 046211.
- [32] A. PIKOVSKY, M. ROSENBLUM, AND J. KURTHS, *Synchronization: A Universal Concept in Nonlinear Sciences*, Cambridge University Press, New York, 2001.
- [33] L. M. RITCHIE, M. A. LOHE, AND A. G. WILLIAMS, *Synchronization of relativistic particles in the hyperbolic Kuramoto model*, Chaos: An Interdisciplinary Journal of Nonlinear Science, 28 (2018), p. 053116.
- [34] F. A. RODRIGUES, K. D. P. THOMAS, P. JI, AND J. KURTHS, *The Kuramoto model in complex networks*, Physics Reports, 610 (2016), pp. 1–98.
- [35] S. STROGATZ, *From Kuramoto to Crawford: exploring the onset of synchronization in populations of coupled oscillators*, Physica D: Nonlinear Phenomena, 143 (2000), pp. 1–20.
- [36] S. STROGATZ, *Exploring complex networks*, Nature, 410 (2001), pp. 268–276.
- [37] S. STROGATZ, *SYNC: The Emerging Science of Spontaneous Order*, Penguin Adult, New York, NY, 2004.
- [38] M. THÜMLER, S. G. SRINIVAS, M. SCHRÖDER, AND M. TIMME, *Synchrony for weak coupling in the complexified Kuramoto model*, Physical Review Letters, 130 (2023), p. 187201.
- [39] J. VAN HEMMEN AND W. WRESZINSKI, *Lyapunov function for the Kuramoto model of nonlinearly coupled oscillators*, Journal of Statistical Physics, 72 (1993), pp. 145–166.
- [40] A. T. WINFREE, *Biological rhythms and the behavior of populations of coupled oscillators*, Journal of Theoretical Biology, 16 (1967), pp. 15–42.